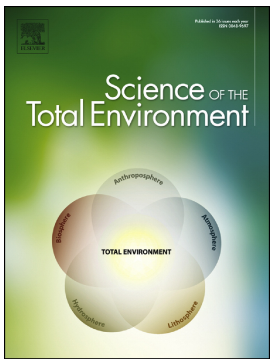

Geoenvironmental Properties of Industrially Contaminated Site Soil Solidified/Stabilized with a Sustainable By-product-based Binder

Ya-Song Feng, Yan-Jun Du, Annan Zhou, Ming Zhang, Jiang-Shan Li, Shi-Ji Zhou, Wei-Yi Xia

PII: S0048-9697(20)36307-5

DOI: https://doi.org/10.1016/j.scitotenv.2020.142778

Reference: STOTEN 142778

To appear in: *Science of the Total Environment*

Received date: 30 August 2020

Revised date: 27 September 2020

Accepted date: 29 September 2020

Please cite this article as: Y.-S. Feng, Y.-J. Du, A. Zhou, et al., Geoenvironmental Properties of Industrially Contaminated Site Soil Solidified/Stabilized with a Sustainable By-product-based Binder, *Science of the Total Environment* (2020), https://doi.org/10.1016/j.scitotenv.2020.142778

Geoenvironmental Properties of Industrially Contaminated Site Soil Solidified/Stabilized with a Sustainable By-product-based Binder

Ya-Song Feng
Ph.D. Student, Jiangsu Key Laboratory of Urban Underground Engineering and Environmental Safety, Institute of Geotechnical Engineering, Southeast University, Nanjing 211189, China. Email: fengyasong@seu.edu.cn

Yan-Jun Du*
Professor, Jiangsu Key Laboratory of Urban Underground Engineering and Environmental Safety, Institute of Geotechnical Engineering, Southeast University, Nanjing 211189, China. (*Corresponding author). Tel: +86-25-83793729, Fax: +86-25-83795086. Email: duyanjun@seu.edu.cn

Annan Zhou
Associate Professor, Civil and Infrastructure Engineering, School of Engineering, Royal Melbourne Institute of Technology (RMIT), Melbourne, Vic 3000, Australia. Email: annan.zhou@rmit.edu.au

Ming Zhang
Professor, Geological Survey of Japan, National Institute of Advanced Industrial Science and Technology (AIST), 1-1-1, Higashi, Tsukuba, Ibaraki 305-8567, Japan. Email: m-zhang@aist.go.jp

Jiang-Shan Li
Professor, State Key Laboratory of Geomechanics and Geotechnical Engineering, Institute of Rock and Soil Mechanics, Chinese Academy of Sciences, Wuhan 430071, China. Email: jsli@whrsm.ac.cn

Shi-Ji Zhou
Ph.D. Student, Jiangsu Key Laboratory of Urban Underground Engineering and Environmental Safety, Institute of Geotechnical Engineering, Southeast University, Nanjing 211189, China. Email: shijizhou@seu.edu.cn

Wei-Yi Xia
Postdoctoral Researcher, Jiangsu Provincial Academy of Environmental Science, Nanjing 210036, China. Email: xiaweiyi@seu.edu.cn

Revised paper submitted to ***Science of the Total Environment***

Abstract: This paper presents a study on utilizing a novel BCP binder, basic oxygen furnace slag (BOFS) activated with mixed calcium carbide residue (CCR) and phosphogypsum (PG), to solidify/stabilize heavy metals in industrial contaminated site soil. The effects of curing time and binder dosage on the geoenvironmental properties of the solidified/stabilized soil including soil pH, electrical conductivity, unconfined compressive strength, and leachability were tested and discussed. Chemical speciation of target heavy metals, pore-size distribution of treated soil, and phase identification of reaction products were analyzed to understand the mechanisms leading to the change of geoenvironmental properties. The results demonstrated that the addition of the BCP binder yielded remarkable increase in soil pH, unconfined compressive strength, and relative binding intensity index (I_R) of target heavy metals including nickel (Ni) and zinc (Zn), while significantly decreased the electrical conductivity and leachability of contaminated soil. The I_R value of heavy metals had a good linear relationship with the leached concentrations on a semi-logarithmic scale. The formation of heavy metal-bearing precipitates, absorptivity of calcium silicate hydrate (C-S-H), heavy metals encapsulation by C-S-H, and ion-exchange of heavy metals with ettringite (AFt) contributed to the immobilization of heavy metals in the solidified/stabilized soil.

Keywords: Contaminated soil, Heavy metal, By-products, Solidification/stabilization, Leachability, Unconfined compressive strength.

1. Introduction

Since the 1980s, a large number of industrial enterprises have moved from mega city to suburban areas because of the nationwide adjustment of urban layout in China (Du et al., 2014; Yang et al., 2018; Zhou and Liu, 2018). The soil contamination at abandoned industrial sites is of increasing concern because of its potential threat to public health and detrimental effects on ecosystems (Feng et al., 2018; Zhou and Wang, 2019; Xia et al., 2019; Du et al., 2020) Accordingly, effective remediation strategy is in a high demand to improve the

ecological environment quality of the contaminated soils so as it can be reused as sustainable construction materials.

Solidification/stabilization is widely used for treating heavy metal-contaminated soils and Portland cement (PC) is the most popular binder used in previous studies and engineering practice (Sharma and Reddy, 2004; Spence and Shi, 2004; Du et al., 2014; Tian et al., 2019; Zhang et al., 2020). However, PC manufacturing consumes large amounts of energy and emits high levels of greenhouse gas. It is reported that the PC industry accounts for 15% of total energy consumption in the industrial sector and contributes as much as 5% to 10% of global anthropogenic CO_2 emissions (Ansari and Seifi, 2013; Mikulčić et al., 2016; Li et al., 2020). Furthermore, PC plants are traditionally characterized as an intensive consumer of unrenewable natural materials such as limestone, clay minerals, and fossil fuels (Hasanbeigi et al., 2012). Researchers have been exploring the potential application of various by-products for alternatives, such as ground granulated blast furnace slag, fly ash, spent coffee grounds, construction and demolition materials, red mud, paper ash, and so on (Horpibulsuk et al., 2009; Rahman et al., 2015; Kua et al., 2016; Hua et al., 2017; Ma et al., 2017; Phummiphan et al., 2018; Kurda et al., 2018; Wu et al., 2018; Jiang et al., 2018; Chen et al., 2019; Gollakota et al., 2019; Dong et al., 2020; Oprkal et al., 2020; Wu et al., 2020). However, very limited researches have investigated the application of basic oxygen furnace slag (BOFS) in solidification/stabilization of heavy metals in industrially contaminated soils.

BOFS is a by-product generated from the conversion process of iron to steel in a basic oxygen furnace, the amount of BOFS accounts for 10% to 15% of produced basic oxygen furnace steel (Shi, 2004; Proctor et al., 2006; Poh et al., 2006). In China, more than 400 million tons of steel slag (mainly BOFS) is deposited per annum, and the amount is continually increasing at a rate of about 100 million tons annually (Zhang et al., 2011). It is reported that the mineral phases of BOFS are dicalcium silicate (C_2S, including β-C_2S and γ-C_2S) and tricalcium

silicate (C_3S) which are also known as major contributors to strength development of PC (Shi, 2004; Zhang et al., 2011). Thus, the BOFS can be potentially used as a substitute to PC in preparing a binder for environmental and economic benefits. However, the β-C_2S formed in BOFS have less hydration activity compared with those in the cement clinker due to their larger crystal size resulted from higher operating temperature (~100 °C) in the basic oxygen furnace (Shi, 2004; Poh et al., 2006). Hence, hydrated BOFS paste and BOFS solidified/stabilized uncontaminated soil show low strength, especially at the early curing stage (Poh et al., 2006; Zhang et al., 2011). On the other hand, the acceleration of the hydration of BOFS by chemical admixtures has been studied by many researchers. The commonly used admixtures are cement clinker, quicklime (CaO), gypsum ($CaSO_4 \cdot 2H_2O$), and calcium chloride ($CaCl_2$) (Poh et al., 2006; Zhang et al., 2011; Belhadj et al., 2012), which come from non-renewable resources. Therefore, the attempt of searching by-product-based admixtures containing these components (i.e., CaO, $CaSO_4 \cdot 2H_2O$, and $CaCl_2$) is a feasible way to make the BOFS-based binder more economical and environment-friendly.

Calcium carbide residue (CCR) is a by-product of polyvinyl chloride, polyvinyl alcohol, and acetylene production. The dominant components of CCR are calcium hydroxide ($Ca(OH)_2$), limited amounts of calcium carbonate ($CaCO_3$), and silicon dioxide (SiO_2) (Jiang et al., 2015; Du et al., 2016). In addition, phosphogypsum (PG) is an industrial by-product of phosphoric acid from natural phosphate rock by the wet process. PG is mainly composed of gypsum ($CaSO_4 \cdot 2H_2O$) and some impurities such as phosphates, fluorides, and sulphates (Rashad, 2017). Hence, the application of mixed CCR and PG to activate BOFS paste is feasible, as the presence of $Ca(OH)_2$ and $CaSO_4 \cdot 2H_2O$ can effectively enhance the hydration reaction of the silicates contained in BOFS (Poh et al., 2006; Zhang et al., 2011). The expected hydration products including calcium silicate hydrate (C-S-H), ettringite (AFt), and portlandite

($Ca(OH)_2$) can facilitate the improvement of soil strength by the cementation and soil pore filling effects of these products. Furthermore, the formation of metal-bearing hydroxides, the absorptivity of C-S-H, heavy metals encapsulation by C-S-H, and the ion-exchange of heavy metals with AFt can result in the immobilization of heavy metals in the solidified/stabilized soil matrix (Sharma and Reddy, 2004; Spence and Shi, 2004; Du et al., 2014). However, studies on assessing the feasibility of BOFS activation by mixed CCR and PG are not available in the literature. Moreover, no existing research addressed the effectiveness and mechanisms of using mixed CCR and PG activated BOFS to solidify/stabilize contaminated soil with a relatively high concentration of heavy metals.

To evaluate the effectiveness of solidification/stabilization, the leachability and strength of the solidified/stabilized soils are the most persuasive geoenvironmental properties (Sharma and Reddy, 2004; Spence and Shi, 2004; Du et al., 2014). Mercury intrusion porosimetry (MIP) is a technique to characterize the microporosity structure of soils, which provides important information in understanding the soil strength and evaluating the pores-filling effects within the soils solidified/stabilized with various binders such as PC, quicklime, and other novel binders (Horpibulsuk et al., 2009; Li and Zhang, 2009; Du et al., 2014; Jiang et al., 2015; Cai et al., 2019a). X-ray diffraction (XRD) and scanning electron microscope (SEM)-energy dispersive spectroscopy (EDS) analyses are extensively used to investigate microstructural and phase information of reaction products in hydrated binder pastes and solidified/stabilized soils, which are responsible for the macroscopic change of the geoenvironmental properties of the solidified/stabilized soils such as the reduction in leachability and increase in soil strength (Du et al., 2014; Jiang et al., 2015; Xia et al., 2019; Cai et al., 2019b). Furthermore, chemical speciation distribution of heavy metals obtained by European Communities Bureau of Reference sequential extraction procedure (BCR SEP) is reported to significantly influence

the leached concentrations of heavy metals in solidified/stabilized soils (Xia et al., 2019). However, the relationship between the leachability and chemical speciation distribution of heavy metals has not been well addressed.

The objectives of this study are to (1) assess the feasibility of utilizing the novel type of BOFS-CCR-PG binder named as BCP binder to immobilize Ni and Zn in a typical electroplating industrial site soil, (2) evaluate the effects of curing time and binder dosage on the primary geoenvironmental properties of the solidified/stabilized soil (e.g., the leachability and strength), and (3) investigate the mechanisms responsible for the changes in the abovementioned geoenvironmental properties with BCR SEP (chemical speciation distribution of heavy metals obtained by European Communities Bureau of Reference sequential extraction procedure), MIP (Mercury intrusion porosimetry), XRD (X-ray diffraction), and SEM-EDS (scanning electron microscope - energy dispersive spectroscopy) analyses. The results facilitate the application of BCP in solidification/stabilization of heavy metal-contaminated soils.

2. Materials and test programs

2.1. Materials

A real site soil collected from a decommissioned electroplating plant in Nantong City, China was used in this study. During the past 60-year operation, the shallow ground soil at the post electroplating plant was contaminated with high concentrations of nickel (Ni) and zinc (Zn). The site investigation report indicated that the Ni concentration of the contaminated soil in the depth of 0-50 cm exceeded the risk intervention value (2000 mg/kg) prescribed in China GB 36600 (China MEE and China GAQSIQ, 2018). Hence, the soil remediation depth at this site was designed to be 50 cm. Surface soil excavated within a depth of 50 cm was collected,

stored in polyethylene bags and transported to the laboratory. The oven-dried soil was then crushed, passed through a 2-mm sieve, and stored in sealed bags for subsequent engineering properties and environmental characteristics tests and the measured values are summarized in Table 1.

The BCP binder developed in this study is a mixture of BOFS, CCR, and PG in a dry mass ratio of 6:3:1, as this ratio yielded relatively low leached concentrations of heavy metals and high strength of the solidified/stabilized soil in the preliminary tests conducted by authors. The fresh BOFS collected from a local steel factory was air-dried and then subjected to mechanical grinding to increase its specific surface area (SSA). In general, the hydration activity of BOFS can be improved with increasing SSA (Proctor et al., 2006; Shi, 2004), but the grinding treatment is very time/cost-consuming. Preliminary tests were conducted to investigate the effect of the SSA of BOFS on the solidified/stabilized efficiency. The test results indicated that when the SSA of BOFS is higher than 300 m^2/kg, there was insignificant reduction in the leached concentrations of heavy metals or enhancement of strength of solidified/stabilized soil. Hence, the SSA of BOFS was determined to be 300 m^2/kg in this study. The dry CCR and PG powders purchased from a by-product recycling company were grounded to pass through a 0.25-mm sieve. The physicochemical properties and chemical compositions of BOFS, CCR, and PG are shown in Tables 2 and 3. Before mixing with contaminated soil, the binder was prepared by dry-mixing the raw materials in the designed proportions using an electric mixer for 30 min to achieve homogeneity.

2.2. Sample preparation

The standard Proctor compaction tests were conducted to obtain the maximum dry density (ρ_{max}) and optimum water content (w_{opt}) of the binder admixed soils immediately after

sufficient mixing. The preliminary test results showed that the ρ_{max} and w_{opt} of the admixed soils with 4%, 6%, 8%, and 10% of binder dosages were 16.5%, 15.2%, 17.3%, 17.6%, and 1.71, 1.79, 1.81, 1.86 g/cm^3, respectively. The binder dosage (or water content) is defined as the weight ratio of the binder (or water) to the oven-dried contaminated soil.

Table 4 summarizes the binder dosage and curing time for various tests. To prepare admixed soil samples for unconfined compressive strength (UCS), soil pH, soil electrical conductivity (EC), and leaching toxicity tests, a predetermined amount of binders (i.e., 4%, 6%, 8%, and 10%) and deionized water (corresponding to w_{opt} of the solidified/stabilized soils, respectively) were added into the oven-dried soils. Then, the mixtures containing soil, water, and binder were thoroughly stirred using an electric mixer for 10 min to achieve homogeneity. A predetermined amount of admixed soil was then transferred into a stainless-steel cylindrical mold with a diameter of 50 mm and a height of 100 mm, and statically compacted using a hydraulic jack to obtain the desired dry density (i.e., 95% of the ρ_{max}). The cylindrical soil samples (Φ 50 mm×H 100 mm) were carefully extruded from the mold, sealed in a polyethylene bag, and cured in a standard curing room (temperature of 20±2 °C and relative humidity of 95%). The solidified/stabilized soil samples were prepared in triplicate for UCS, soil pH, soil EC, and leaching tests.

2.3. UCS, pH, EC and leaching tests

After designed curing time, the as-hydrated soil samples were taken out from the standard curing room and immediately used for UCS tests. Then triplicate 10 g of subsamples retrieved from the broken UCS test samples were employed for soil pH, soil EC, and leaching tests. The solidified/stabilized soil samples were subjected to unconfined compression test with the strain rate controlled at 1%/min as per ASTM D4219 (ASTM, 2017). The soil pH

measurement was conducted using a HORIBA D-54 pH meter as per ASTM D4972 (ASTM, 2019). The soil EC was measured using a DDS-22C conductivity meter as per JGS 0212 (JGS, 2010). The leaching tests were conducted as per China HJ/T 299 (China MEP, 2007).

2.4. BCR SEP and MIP tests

The preparation method of soil samples for BCR SEP and MIP tests was the same as that of the soil samples for UCS, soil pH, and leaching tests. Approximately 10 g of powder subsample for BCR SEP and 1 cm^3 of cube subsample for MIP test were carefully collected from a hand-broken cylindrical soil sample. Prior to BCR SEP and MIP tests, these soil subsamples were frozen using liquid nitrogen and then dried in a vacuum chamber by sublimation of the frozen water at a temperature of -30 °C. One solidified/stabilized soil sample was prepared for BCR SEP or MIP test.

The BCR SEP was performed with the same procedures provided by Davidson et al. (1998) for determining the exchangeable, reducible, oxidizable, and residue fractions of Ni and Zn in the soil samples. To quantitatively describe the chemical stability of heavy metals of the BCP solidified/stabilized soil by one variable, the relative binding intensity index (I_R) is used in this study. The I_R is used to evaluate the mobility of trace metals contained in soils, composts, and sediments (Han et al., 2003; Gusiatin et al., 2014), and defined as Eq. (1):

$$I_R = \sum_{i=1}^{k} (F_i i^n) / k^n \quad (1)$$

where, i is the number of the extraction steps, progressing from 1st (for the weakest) to the strongest extractant used in the kth step (k is 4 in the BCR procedure adopted in this study); F_i is the percentage of a particular trace metal presented in fraction i, and n is 1 or 2 as proposed in previous studies by Han et al. (2003) and Gusiatin et al. (2014). A higher I_R value of a given heavy metal element represents a more stable pattern of the speciation distribution and

more quantity of metal residues in the soil and vice versa.

The MIP test was performed using an AutoPore IV 9510 mercury intrusion porosimeter capable of generating pressure in the range of subambient to 413 MPa. The pore diameter was calculated using the following capillary pressure equation (Mitchell and Soga, 2005):

$$d = -\frac{4\tau \cos\alpha}{p} \tag{2}$$

where d is the pore entry diameter in which mercury is being intruded (μm), τ is the surface tension (N/m), α and p are the contact angle of mercury with the soil (°) and applied pressure of mercury intrusion (MPa), respectively. In this study, the surface tension and contact angle at 25 °C were assigned to be 139° and 4.84×10^{-4} N/m, as suggested by Wu et al. (2018).

Peak analysis is widely adopted to quantitatively evaluate the pore distribution characteristic of the solidified/stabilized soils, and Gaussian distribution functions are commonly applied to fit each peak of the PSD scatterplots (Li and Zhang, 2009; Du et al., 2014). The typical Gaussian distribution function can be written as (Du et al., 2014):

$$f(d) = \sum_{i=1}^{n} f_i(d) = \sum_{i=1}^{n} A_i \frac{1}{\sqrt{2\pi}\sigma_i} e^{-\left[\frac{(\log d - \mu_i)^2}{2\sigma_i^2}\right]} \tag{3}$$

where n is the number of peaks in fitting curves on a logarithmic scale (1 and 2 for the unimodal and bimodal types, respectively), A_i is pore volume in the 1 g dry soil covered by the fitted curve of $f_i(d)$ (mL/g), σ_i is standard deviation on a logarithmic scale, and μ_i is the mean pore diameter in the fitted curve of $f_i(d)$ on a logarithmic scale (μm).

2.5. XRD and SEM-EDS analysis

The formation of $Ni(OH)_2$ or $Zn(OH)_2$ is one of the primary mechanisms of immobilizing Ni or Zn in the cement solidified/stabilized soils (Spence and Shi, 2004). In addition, the

presence of sulfate (SO_4^{2-}) and iron (Fe, exists in tri-valence) had noticeable impacts on the immobilization efficiency of Ni due to the formation of Ni-Fe layered double hydroxides (Ni-Fe LDHs) (Constantino et al., 1995; Li et al., 2010; Wang et al., 2016; Krehula et al., 2018). Meanwhile, the presence of chloride (Cl^-) contributes to the formation of $Zn_5(OH)_8Cl_2 \cdot H_2O$ whose chemical stability is higher than that of $Zn(OH)_2$ (Srivastava and Secco, 2011; Feng et al., 2018). Therefore, it is important to investigate the effects of coexisting chloride (Cl^-), sulfate (SO_4^{2-}), and iron (Fe, exists in tri-valence) on the immobilization of Ni and Zn in the BCP solidified/stabilized soils, as Cl^- and SO_4^{2-} are commonly encountered in the electroplating industrial site soils. When the binder dosage was low and consequently the contaminant-bearing products formed in solidified/stabilized soils were trace, researchers suggested to use heavy metal spiked pastes to investigate the products due to the chemical reactions between hydrated binders and heavy metals (Du et al., 2014; Xia et al., 2017). Hence, in this study, XRD and EDS-mapping analyses were conducted to identify the products formed in the binder pastes with the presence of Fe and mixture of Fe, Cl^-, and SO_4^{2-}.

A series of BCP paste samples spiked by Ni, Zn, Fe, Cl^-, and SO_4^{2-} were prepared for XRD and SEM-EDS analyses. Because the solidified/stabilized soil with a binder dosage of 8% and curing time of 28 d can meet China criterion for groundwater quality of Class IV prescribed in GB/T 14848 (China GAQSIQ and China SA, 2017) (see 3.2 section), the curing time and ratio of binder to contaminants in this soil sample were selected as the prototype of the BCP paste preparation. The concentrations of Ni, Zn, Fe, Cl^-, and SO_4^{2-} in this soil sample were 6053 mg/kg (0.6053%), 5352 mg/kg (0.5352%), 7515 mg/kg (0.7515%), 3735 mg/kg (0.3735%), and 1630 mg/kg (0.1630%) as shown in Table 1. To be consistent with these ratios, a series of BCP binder paste samples were prepared by spiking powder binders with

$Ni(NO_3)_2 \cdot 5H_2O$, $Zn(NO_3)_2 \cdot 5H_2O$, $Fe(NO_3)_3 \cdot 9H_2O$, Na_2SO_4, and NaCl powder (analytical reagent). The mass ratios of Ni, Zn, Fe, Cl^-, and SO_4^{2-} to the dry BCP binder were calculated to be approximately 7.6 (0.6053%:8%), 6.7 (0.5352%:8%), 9.4 (0.7515%:8%), 4.7 (0.3735%:8%), and 2.0 (0.1630%:8%), respectively.

The preparation method of the paste sample was as follows: Firstly, a predetermined amount of $Ni(NO_3)_2 \cdot 5H_2O$, $Zn(NO_3)_2 \cdot 5H_2O$, $Fe(NO_3)_3 \cdot 9H_2O$, Na_2SO_4, and NaCl powders were poured into the dry binder powder in a beaker, and the mixture was thoroughly mixed using a glass stirring rod. Then, predetermined volume of deionized water was slowly added into the mixture to achieve a solid-liquid ratio of 1.0:0.8 (mg: mL), following which the wetted mixture was stirred thoroughly for 10 min to achieve homogeneity. The ratio was to guarantee the thorough mixing of wetted mixture and sufficient reactions that occurred in the wetted mixture. After that, the mixture was poured into a polyethylene mold (inner diameter 50 mm and height 50 mm), top sealed and subjected to curing under the standard condition (temperature of 20±2 °C and relative humidity of 95%) for 7 d. The paste sample was then removed from the mold, sealed in a plastic bag, and cured under the standard condition (temperature of 20±2 °C and relative humidity of 95%) for 21 d. After that, the paste samples were carefully crushed using a rubber hammer. Approximately 1 cm^3 of subsample with fresh surface was immediately collected from each crushed paste sample and frozen-dried. The paste sample was frozen using liquid nitrogen and then dried in a vacuum chamber by sublimation of the frozen water at a temperature of -80 °C. After that, the dried paste sample was ground, sieved through a 200-mesh sieve, and subjected to XRD and SEM-EDS analysis. Samples were designated as BCP+Ni+Zn, BCP+Ni+Zn+Fe, and BCP+Ni+Zn+Fe+ SO_4^{2-}+Cl^- to represent paste samples spiked by the mixture of Ni and Zn, mixture of Ni, Zn, and Fe, mixture of Ni, Zn, Fe, SO_4^{2-}, and Cl^-, respectively (Table 5). One spiked paste sample was

prepared for XRD or SEM-EDS analyses.

After the primary reaction products had been identified by XRD and SEM-EDS analyses conducted on binder pastes, XRD analysis was also conducted on soil samples to investigate the effects of curing time and binder dosage on the formation and quantities of the reaction products. The preparation method of soil samples for XRD analysis was the same as that of the soil samples for UCS, soil pH, and leaching tests. Approximately 10 g of subsample for XRD analysis was carefully collected from a hand-broken cylindrical soil sample, frozen-dried, grounded and sieved through a 200-mesh sieve. The method used to freeze-dry the soil sample was the same as that to freeze-dry paste sample. One solidified/stabilized soil sample was prepared for XRD analysis.

The paste samples and soil samples were scanned over the 2θ range of 5° to 60° for XRD spectra using a Rigaku D/Max-2500 X-ray diffractometer with Cu-Kα radiation. The instrument was operated at 15 kV input voltage and 20 mA current in the step scan mode. The scan time of 5 s was used at each step (0.02°). The gold-coated paste sample was scanned using a LEO 1530VP scanning electron microscope (SEM) to obtain micrographs. Moreover, energy dispersive spectroscopy (EDS) was performed in combination with SEM to characterize the elemental mapping.

2.6. Benchmarking

For comparison, the untreated contaminated soil sample without binder addition (i.e., 0% dosage) and clean BCP paste sample were used to prepare the benchmarking samples. The preparation method of the untreated soil samples was identical to those of the solidified/stabilized soil samples. Meanwhile, the preparation method of the clean BCP paste

sample was identical to those of the spiked BCP paste samples except that no contaminants were added into the bender paste.

Same as the solidified/stabilized soil samples or spiked paste samples, the untreated soil were prepared in triplicate for UCS, soil pH, soil EC, and leaching tests. Untreated soil sample (one specimen) was also prepared for BCR SEP, MIP test, and XRD analysis. One clean paste sample was prepared for XRD analysis. The untreated contaminated soil samples and uncontaminated BCP paste samples were also cured in a standard curing room (temperature of 20±2 °C and relative humidity of 95%).

3. Results and analysis

3.1 Soil UCS, pH, and EC

Fig. 1 shows the variations of soil unconfined compressive strength (UCS), pH, and electrical conductivity (EC) with different curing time and binder dosages. The average values of these triplicate values are reported here. The error bars representing the standard deviations are also plotted in the corresponding figures. The coefficient of variation (COV) is below 5% demonstrating the excellent reproducibility of the test results. It is seen from Fig. 1(a) that, as compared to the compacted untreated soil (i.e., no binder addition), the UCS of the solidified/stabilized soil increases considerably with extending curing time regardless of the binder dosage. This increase is mainly attributed to the time-dependent hydration reaction of the silicates (i.e., C_2S and C_3S) contained in the BCP binder and the simultaneously occurred pozzolanic reaction in the solidified/stabilized soil matrix (Poh et al., 2006; Jiang et al., 2015). The UCS of the solidified/stabilized soil increases with increasing binder dosage, which is due to the presence of more additional products (i.e., calcium silicate hydrate (C-S-H), ettringite (AFt), portlandite ($Ca(OH)_2$), and heavy metal-bearing precipitates addressed in 3.5

section) that exhibit excellent cementation strength between soil particles and filling effects within the soil pores (Shi, 2004; Jiang et al., 2015). A minimum UCS value of 350 kPa has been recommended by the USEPA for the solidified/stabilized materials to be disposed of in a landfill (USEPA, 1996). To meet the USEPA recommend value, as shown in Fig. 1(a), either 8% BCP with 60-d curing or 10% BCP with 14-d curing can be selected to solidify/stabilize soils.

At the early curing period (i.e., 7 d), significant increment in soil pH was observed with the binder addition into the contaminated soil (Fig. 1(b)), owing to the immediate dissolution of the alkaline constituents such as C_2S, C_3S and $Ca(OH)_2$ contained in the BCP binder. However, after the first increase stage, the soil pH decreased gradually with increasing curing time. The phenomenon is attributed to the evolution of pozzolanic reaction in the solidified/stabilized soil matrix and precipitation reaction of heavy metal-bearing hydroxides (i.e., $Ni(OH)_2$ and $CaZn_2(OH)_6{\cdot}2H_2O$), in which a certain amount of hydroxide ion (OH^-) are consumed. Furthermore, the soil EC decreases dramatically with increasing curing time (see Fig. 1(c)), which consequently results in a remarkable decrease in soil salinity.

3.2 Leaching toxicity

Fig. 2 depicts the variation of leached concentrations of heavy metals from BCP solidified/stabilized soil at different curing time and binder dosages. The leached concentrations of Ni and Zn in the untreated contaminated soil are 8.50 and 9.27 mg/L, which significantly exceed the China criterion for groundwater quality of Class IV (0.10 mg/L for Ni and 5.00 mg/L for Zn) prescribed in GB/T 14848 (China GAQSIQ and China SA, 2017). While, the leached concentrations of Ni and Zn from the solidified/stabilized soil sharply decrease with the addition of BCP binder. In addition, the increased curing time and binder

dosage noticeably reduce the concentrations of Ni and Zn leached from the solidified/stabilized soil. The phenomenon is primarily attributed to the time- or dosage-dependent hydration reaction of silicates contained in BOFS, pozzolanic reaction occurred between the dissolved silica dioxide in the soil and the calcium hydroxide from CCR and hydrated BOFS, precipitation reaction of heavy metals, and adsorption of C-S-H that formed in the solidified/stabilized soil matrix. Longer curing time or higher binder dosage enhances the abovementioned reactions, and consequently reduces leached concentrations of heavy metals in the solidified/stabilized soil. This finding is verified based on the chemical speciation distribution of heavy metals presented in 3.3 section.

The test results in Fig. 2 show that 10% and 8% BCP solidified/stabilized soils after curing time of 7 d and 28 d, respectively, meet the China criterion for groundwater quality of Class IV. Previous studies indicated that the hydration and pozzolanic reactions occurred in the soil solidified/stabilized with reactive magnesia activated ground granulated blast furnace slag were slower than the acid-base reaction occurred in soils solidified/stabilized with phosphate-based binders (e.g., KMP binder which consists of monopotassium phosphate, reactive magnesia, and oxalic acid-activated phosphate rock power, and SPC binder which consists of superphosphate and calcium oxide) (Feng et al., 2018; Xia et al., 2019). Hence, it is recommended to appropriately extend the curing time in the soil remediation practice if relatively low BCP dosage is required.

3.3 Heavy metal speciation

Figs. 3 and 4 illustrate the variation of chemical speciation of Ni and Zn in solidified/stabilized soil, respectively. The acid soluble fraction (F1) and residual fraction (F4) remarkably vary with increasing curing time or binder dosage, while the changes in reducible

fraction (F2) and oxidizable fraction (F3) of Ni and Zn are not significant. All the changes in the four fractions have effects on the chemical stability of Ni and Zn in the BCP solidified/stabilized soil and environmental quality of the BCP solidified/stabilized soil (Han et al., 2003).

To analyze the effects of curing time and binder dosage on the chemical stability of heavy metals in the BCP solidified/stabilized soil, I_R values of Ni and Zn calculated by Eq. (1) are shown in Fig. 5. It is seen that the I_R values of Ni and Zn considerably increase with increasing curing time or binder dosage. The results are consistent with those obtained from the leaching tests, in which increasing curing time or binder dosage reduces the concentrations of Ni and Zn leached from the BCP solidified/stabilized soil. The relationship between the I_R values and leached concentrations of Ni and Zn is obtained using a least-square-root method and expressed by the follows:

$$\log C_{Ni}(n) = a \cdot I_R(\mathrm{Ni}) + b \tag{4}$$

$$\log C_{Zn}(n) = c \cdot I_R(\mathrm{Zn}) + d \tag{5}$$

where C_{Ni} or C_{Zn} is the concentration of Ni or Zn leached from the BCP solidified/stabilized soils; n is 1 or 2 as proposed by Han et al. (2003) and Gusiatin et al. (2014); and I_R(Ni) or I_R(Zn) is the relative binding intensity index of Ni or Zn in the BCP solidified/stabilized soil. As shown in Fig. 6, I_R shows a good linear relationship with leached concentrations of heavy metals on a semi-logarithmic scale. Therefore, the reduced leached concentrations of heavy metals with increasing curing time or binder dosage may be attributed to the enhanced I_R values.

3.4 Pore-size distribution

Table 6 indicates the variations of the pore volumes of BCP solidified/stabilized soils. The

total pore volume in 8% BCP solidified/stabilized soil notably decreases from 0.250 to 0.191 mL/g with the curing time extending from 7 to 90 d. On the other hand, when the binder dosage increases from 4% to 10%, the total pore volume in the solidified/stabilized soil after 28 d curing remarkably decreases from 0.255 to 0.183 mL/g. The decrease in voids is owing to the time- or dosage-dependent evolution of reaction products such as C-S-H, AFt, portlandite, and heavy metal-bearing hydroxides that can effectively fill the pore spaces of contaminated soil.

To investigate the variation of pore structures of soils, researchers have divided the pores in these soils into different types based on pore diameter (Li and Zhang, 2009; Horpibulsuk et al., 2009; Khoshghalb et al., 2015; Oualmakran et al., 2016). Following Horpibulsuk et al. (2009), the total pore volume in the BCP solidified/stabilized soil is divided into three types such as intra-aggregate, inter-aggregate, and air pores, with the pore diameters of 0.01 and 10 μm being assigned as thresholds between intra-aggregate and inter-aggregate pores, and inter-aggregate pores and air pores, respectively. As shown in Table 6, when the curing time of 8% BCP solidified/stabilized soil extends from 7 d to 90 d, the inter-aggregate pore volume and air pore volume decrease by 0.051 mL/g and 0.006 mL/g, respectively (the intra-aggregate pore volume of these soils shows negligible change). On the other hand, when the binder dosage of the solidified/stabilized soil with 28 d curing increases from 4% to 10%, the inter-aggregate pore volume and air pore volume decrease by 0.049 mL/g and 0.017 mL/g, respectively (the intra-aggregate pore volume of these soils shows negligible change). The results indicate that the time- or dosage-dependent reduction in the total pore volume in the BCP solidified/stabilized soil primarily results from the reduction in the inter-aggregate pore volume. It is reported that the reduction in inter-aggregate pore volume is the primary reason for the remarkable improvement of the strength of compacted soils treated with PC, fly ash, or

hydroxyapatite-based binder (Horpibulsuk et al., 2009; Du et al., 2014; Xia et al., 2017).

Fig. 7 illustrates the variations of the pore size distribution (PSD) in the BCP solidified/stabilized soils. The Y-axis is plotted as $f(d)$ ($f(d) = \mathrm{d}V/\mathrm{dlog}d$), where V is the volume of pores (mL/g) having a diameter of d (μm) in 1 g of the dry solidified/stabilized soil. Bimodal PSDs are usually observed in compacted solidified/stabilized clayey/slit soil (Horpibulsuk et al., 2009; Du et al., 2014; Xia et al., 2017). From Fig. 7, it is seen that bimodal PSDs are observed in the scatter plotted $f(d)$ of the BCP solidified/stabilized soils at early curing time (i.e., 7 d and 28 d for 8% BCP dosage, see Fig 7(a) and 7(b)) or with few binder dosages (i.e., 4%, 6%, and 8% for 28 d curing, see Fig 7(d), 7(e), and 7(b)). Such bimodal PSDs have also been observed in completely decomposed granitic soil (Li and Zhang, 2009), compacted clean clayey soils (Simms and Yanful, 2001), and PC solidified/stabilized kaolin soil contaminated by Zn with low concentration (< 0.2%) (Du et al., 2014). Furthermore, when the curing time increases to 90 d (see Fig 7(c)) or binder dosage increase to 10% (see Fig 7(f)), these two peaks gradually converge to be one. The bimodal PSD curve was reported to be found in fly ash blended cement stabilized silty clay, carbonated reactive magnesia-admixed silty soil, phosphate-based binder solidified/stabilized clay soil (Horpibulsuk et al., 2009; Cai et al., 2019; Xia et al., 2019). The variation in PSD is because that the some air pores or inter-aggregate pores are filled with and/or separated by the reaction products such as C-S-H, AFt, portlandite, and heavy metal-bearing precipitates, and consequently they transform into inter-aggregate pores or intra-aggregate pores.

Table 7 lists the changes in the parameters of A_i, μ_i, and σ_i when curing time extends from 7 to 90 d for the 8% BCP solidified/stabilized soil samples, and when binder dosage increases from 4% to 10% for BCP solidified/stabilized soil samples at 28 d curing. The fitting

parameters for simulated $f_1(d)$ curve are A_1, μ_1, and σ_1; and for simulated $f_2(d)$ curve are A_2, μ_2, and σ_2, respectively. The PSD of the 8% BCP solidified/stabilized soils with 7 d and 28 d curing are bimodal (see Fig. 7). It is seen that from Table 7, when curing time increases from 7 to 28 d for 8% BCP solidified/stabilized soil samples, μ_1 varies from -0.633 to -0.652 μm, which corresponds to a decrease in the mean diameter of soil pore covered by $f_1(d)$ curve from 0.233 to 0.223 μm (i.e., a 4.28% decrease). Meanwhile, μ_2 for these soil samples drops from -0.287 to -0.582 μm, which corresponds to a notable decrease in the mean diameter of soil pore covered by $f_2(d)$ curve from 0.516 to 0.262 μm (i.e., a 49.2% decrease). On the other hand, when curing time extends from 7 to 28 d, A_1, which corresponds to the volume of the pore covered by the simulated $f_1(d)$ curve, shows a slight reduction by approximately 0.007 mL/g. Meanwhile, A_2 remarkably decreases from 0.045 to 0.026 mL/g. The μ_1 and A_1 for the simulated $f_1(d)$ curve of BCP solidified/stabilized soil with 90 d curing decrease to -0.738 μm and 0.182 mL/g, respectively.

Furthermore, the PSD of 4%, 6% and 8% BCP solidified/stabilized soils with 28 d curing are bimodal (see Fig. 7). From Table 7, it is seen that when binder dosage increases from 4% to 8%, μ_1 and μ_2 decrease from -0.151 to -0.652 μm and 0.892 to 0.203 μm, respectively. Accordingly, the mean diameters of soil pores covered by simulated $f_1(d)$ and $f_2(d)$ curves decrease by 0.483 and 6.202 μm, respectively. Besides, when binder dosage increases from 4% to 8%, A_1 and A_2, which correspond to the volume of the pore covered by the simulated $f_1(d)$ and $f_2(d)$ curve, remarkably decrease by 0.016 and 0.045 mL/g. The μ_1 and A_1 for simulated $f_1(d)$ curve of 10% BCP solidified/stabilized soils continually decrease to -0.916 μm and 0.180 mL/g.

The variation in these fitting parameters listed in Table 7 indicates that with increasing curing

time (28d to 90 d) or binder dosage (4% to 10%), the mean diameter and volume of soil pores gradually decrease with increasing binder dosage and/or curing time. The results agree well with those of Horpibulsuk et al. (2009) and Xia et al. (2019) who studied the effects of binder dosage and curing time on the pore-size distribution characteristic of soils solidified/stabilized by PC, fly ash, and hydroxyapatite-based binder.

3.5 X-Ray diffraction and SEM-EDS analysis of paste samples

Fig. 8 shows X-ray diffractograms of the hydrated BCP paste spiked with various contaminants such as Ni, Zn, Fe, SO_4^{2-}, and Cl^- after 28 d curing. Diffractogram for clean hydrated BCP paste is also presented as a reference. The presence of un-hydrated C_2S, Fe_2O_3, RO phase, and newly generated C-S-H, AFt, and portlandite are identified in all of the paste samples irrespective of the presence of contaminants. Previous studies showed that BOFS has limited hydraulic properties, and hardly any hydration products such as C-S-H, AFt, and portlandite could be detected when exposed to aqueous environment (Shi, 2004; Proctor et al., 2006). With the rapid dissolution of CCR in the porewater of the BCP paste, the high alkaline in the porewater promotes the hydration of the silicates contained in BOFS (Poh et al., 2006; Belhadj et al., 2012). Then the relatively high concentrations of Ca^{2+} and SO_4^{2+} released from PG contribute to the formation of AFt (Shi, 2004). Therefore, the substantial hydration products of C-S-H, AFt, and portlandite presented in the hydrated BCP paste (Fig. 8) indicate that the hydration activity of BOFS is significantly improved by the activation of mixed CCR and PG.

For the BCP paste spiked with mixed Ni and Zn, the presence of α-$Ni(OH)_2$, β-$Ni(OH)_2$, and $CaZn_2(OH)_6 \cdot 2H_2O$ are detected. Furthermore, Ni-Fe layered double hydroxides (Ni-Fe LDHs(C), $[Ni_{1-x}Fe_x(OH)_2]^{x+}(CO_3)_{x/2} \cdot yH_2O$), as well as α-$Ni(OH)_2$, β-$Ni(OH)_2$, and

$CaZn_2(OH)_6 \cdot 2H_2O$ are detected in the BCP paste spiked by the mixture of Ni, Zn, and Fe. When the BCP paste is contaminated with the mixed spikes of Ni, Zn, Fe, SO_4^{2-}, and Cl^-, the presence of α-$Ni(OH)_2$, β-$Ni(OH)_2$, Ni-Fe LDHs(C), $CaZn_2(OH)_6 \cdot 2H_2O$, and $Zn_5(OH)_8Cl_2 \cdot H_2O$ are identified in the hydrated BCP paste.

Fig. 9(a) shows SEM images for the hydrated BCP paste spiked with the mixture of Ni, Zn, Fe, SO_4^{2-}, and Cl^-, and Fig. 9(b) shows the EDS distribution maps for elements of Ni, Zn, Fe, Ca, C, and Cl, respectively. It is seen that the products of α-$Ni(OH)_2$ and β-$Ni(OH)_2$ detected by XRD analysis in the BCP paste spiked with mixed Ni and Zn (Fig. 8), are identified in Fig. 9(a) when overlapping the distribution maps for the elements of Ni and O. The Ni-Fe LDHs(C) is identified by overlapping the distribution maps for the elements of Ni, Fe, O, and C. Meanwhile, when overlapping the distribution maps for the elements of Zn, O, and Ca, the presence of $CaZn_2(OH)_6 \cdot 2H_2O$ is identified, which is also supported by the XRD analysis for the BCP paste spiked with mixed Ni and Zn as shown in Fig. 8. The $Zn_5(OH)_8Cl_2 \cdot H_2O$ highlighted by overlapping the distribution maps for the elements of Zn, O, and Cl is also observed in the BCP paste spiked with the mixture of Ni, Zn, Fe, SO_4^{2-}, and Cl^- by XRD analysis (Fig. 8).

From Fig. 8, it is seen that the primary mechanisms of Ni and Zn immobilization in the BCP paste after 28 d curing are significantly impacted by the presence of Fe and Cl^-, while the presence of SO_4^{2-} is negligible. For instance, compared with the hydrated BCP paste spiked with mixed Ni and Zn, the extra Ni-Fe LDHs(C) and $Zn_5(OH)_8Cl_2 \cdot H_2O$ are detected in the hydrated BCP pastes when the mixture of Ni, Zn, Fe, SO_4^{2-}, and Cl^- is present. The Ni-Fe LDHs(C) is the finally generated Ni-bearing layered double hydroxides (LDHs) in the hydrated BCP paste sample spiked with the mixture of Ni, Zn, Fe, SO_4^{2-}, and Cl^- (see Fig. 8).

However, the Ni-Al layered double hydroxides (Ni-Al LDHs(C), $[Ni_{1-x}Al_x(OH)_2]^{x+}(CO_3)_{x/2}\cdot yH_2O$) is formed in the hydrated cement paste (Vespa et al., 2006). This difference is attributed to (1) the presence of a higher concentration of Fe in the mixture of BCP paste and contaminants than that in the Ni-spiked cement paste tested by Vespa et al. (2006), and (2) the lower solubility of Ni-Fe LDHs(C) (solubility product constant, $K_{sp}=3.11\times10^{-24}$) compared with that of the Ni-Al LDHs(C) ($K_{sp}=4.75\times10^{-22}$) (Johnson and Glasser, 2003; Wang et al., 2016; Krehula et al., 2018). The presence of Zn-bearing product, $Zn_5(OH)_8Cl_2\cdot H_2O$, identified in the BCP paste spiked with the mixture of Ni, Zn, Fe, SO_4^{2-} and Cl^- is due to the lower solubility of $Zn_5(OH)_8Cl_2\cdot H_2O$ ($K_{sp}=2.35\times10^{-17}$) than that of $Zn(OH)_2$ ($K_{sp}=1.80\times10^{-14}$) (Haynes, 2014; Feng et al., 2018).

The mechanisms responsible for immobilization of heavy metals are discussed based on the results obtained from paste samples. The hypotheses are further discussed by exploring the reaction products formed in the BCP solidified/stabilized soil (see 3.6 section).

3.6 X-Ray diffraction analysis of contaminated soil samples

Fig. 10 presents the X-ray diffractograms of the 8% BCP solidified/stabilized soils at 7 d, 28 d, and 90 d curing. Fig. 11 shows the X-ray diffractograms of the solidified/stabilized soils with different binder dosages cured for 28 d. Diffractogram for untreated contaminated soil is also presented as a reference. It is seen from Figs. 10 and 11 that the generated products including C-S-H, AFt, and portlandite observed in the hydrated clean BCP paste (see Fig. 8) are identified in all of the solidified/stabilized soil samples. The C-S-H possesses excellent cementation property between soil particle and AFt or portlandite shows filling effect to soil pores (Jiang et al., 2015; Du et al., 2014). Hence, the formed C-S-H, AFt, and portlandite play an important role in the improvement of soil strength (Fig. 1). Furthermore, the absorptivity

of C-S-H, heavy metals encapsulation by C-S-H, and ion-exchange of heavy metals with AFt partly contribute to the reduced leached concentrations (Fig. 2) and increased chemical stability of heavy metals in the soil (Figs. 3 and 4).

It is also seen from Fig. 10 that, for specific curing time and/or binder dosage, all the Ni- and Zn-bearing products observed in the hydrated BCP paste such as α-$Ni(OH)_2$, β-$Ni(OH)_2$, Ni-Fe LDHs(C), Ni-Fe LDHs(S), $CaZn_2(OH)_6 \cdot 2H_2O$, and $Zn_5(OH)_8Cl_2 \cdot H_2O$ (see Fig. 8) are identified in the solidified/stabilized soil. However, the intermediate product of Ni-Fe LDHs(S) presented in the 8% BCP solidified/stabilized soil sample at 28 d curing is not detected in the hydrated BCP paste (see Fig. 8) or the hydrated cement paste studied by Vespa et al. (2006; 2007). This difference is attributed to that the transformation of Ni-Fe LDHs(S) to Ni-Fe LDHs(C) is only occurred when sufficient amount of carbonate (CO_3^{2-}) is available in the pore solution of the soil (Li et al., 2010). Generally, the higher pH of the pore solution in hydrated BCP paste (Fig. 1) or hydrated cement paste (Vespa et al., 2006) allows sufficient amount of CO_2 from the atmosphere to dissolve into the pore solution and then transforms to CO_3^{2-} at a certain curing time, i.e., 28 d (Li et al., 2010). In other words, the lower pH of the BCP solidified/stabilized soil hinders the transformation of Ni-Fe LDHs(S) to Ni-Fe LDHs(C) in 28 d curing age, which is due to the absence of sufficient amount of dissolved CO_2 in the soil pore solution. For example, the respective pH values are 10.5 and 11.3 for the 8% BCP solidified/stabilized soil sample and hydrated BCP paste sample at 28 d curing (see Fig. 1). Furthermore, with curing time extending to 90 d, the Ni-Fe LDHs(S) gradually transforms to Ni-Fe LDHs(C), which is resulted from the progressive dissolution of CO_2 in the pore solution and consequently sufficient amount of CO_3^{2-} presented in the pore solution of contaminated soil. The transformation of crystalline phase of Ni-bearing LDHs, to some extent, contributes to the improvement of chemical stability of Ni (Fig. 3(a)) and the reduction

in the leached concentration of Ni ((Fig. 2(a)).

It is interesting to note that, however, the presence of Ni-Fe LDHs(C) is only identified in the case of 50% BCP addition at 28 d curing (see Fig. 11). This phenomenon is attributed to the higher pH of the solidified/stabilized soil with a higher binder dosage (50%). For instance, the pH value of the solidified/stabilized soil with 50% BCP dosage after 28 d curing is 12.7, while the pH values are 10.5 and 11.6 for 8% and 20% BCP dosage, respectively. Similar to the case of the time-dependent phase transformation of LDHs in the solidified/stabilized soil, the higher pH of the 50% BCP solidified/stabilized soil allows sufficient amount of CO_2 to dissolve into the pore solution and result in the formation of Ni-Fe LDHs(C) (Li et al., 2010). The presence of α-$Ni(OH)_2$ and β-$Ni(OH)_2$, corresponding to two-theta of 11.36° and 19.26°, are detected in all soil samples with 8%, 20%, and 50% BCP addition (Fig. 11). Furthermore, the presence of Ni-Fe LDHs(S), $CaZn_2(OH)_6 \cdot 2H_2O$, and $Zn_5(OH)_8Cl_2 \cdot H_2O$ are identified in all the solidified/stabilized soils.

Tables 8 and 9 summarize the primary hydration products of BCP and heavy metal-bearing products observed in the BCP solidified/stabilized soils and the corresponding peak intensity of these concerned products. It is found that the peak intensity exhibits different variation trend with increasing curing time or binder dosages. For instance, the peak intensity of C-S-H, AFt, and portlandite gradually increases with increasing curing time or binder dosage. The accumulation of C-S-H, AFt, and portlandite leads to the gradual reduction in pore volumes of the solidified/stabilized soil (Table 6) but improvement of soil strength (Fig. 1).

From Table 8, it is also found that the peak intensity of α-$Ni(OH)_2$ ($K_{sp}=5.48\times10^{-16}$) in the case of 28 d curing is weaker than that in the case of 7 d curing, and no obvious peak

corresponding to α-Ni(OH)$_2$ at 90 d curing is detected in the solidified/stabilized soil sample. In contrast, the development of β-Ni(OH)$_2$ (K_{sp}=7.92×10^{-17}) exhibits an opposite trend as compared with that of α-Ni(OH)$_2$. In other words, the peak corresponding to β-Ni(OH)$_2$ in the solidified/stabilized soil samples is not detected until 28 d curing, after which the peak intensity continuously increases with extending curing time. This phenomenon indicates that α-Ni(OH)$_2$ is the early Ni-bearing product, and then it gradually transforms into β-Ni(OH)$_2$ and Ni-Fe LDHs as the chemical stability of β-Ni(OH)$_2$ (K_{sp}=7.92×10^{-17}) and Ni-Fe LDHs (K_{sp}=3.11×10^{-24}) is higher than that of α-Ni(OH)$_2$ (K_{sp}=5.48×10^{-16}) (Vespa et al. 2006; Haynes, 2014; Krehula et al., 2018). The change pattern of these Ni-bearing products formed in the BCP solidified/stabilized soil sample is the same as that in the Ni-spiked cement paste reported in Vespa et al. (2006; 2007), in which the time-dependent phase transformation of Ni-bearing products in hydrated cement paste doped with Ni was studied. The peak intensity of $CaZn_2(OH)_6{\cdot}2H_2O$ has no significant variation with increasing curing time. Meanwhile, the peak intensity of $Zn_5(OH)_8Cl_2{\cdot}H_2O$ increases with extending curing time (see Table 8).

It is found from Table 9 that the peak intensity corresponding to all the heavy metal-bearing products markedly increases with increasing binder dosage, suggesting the dosage-dependent accumulation of these products in the BCP solidified/stabilized soil.

In summary, the time- or dosage-dependent accumulation of reaction products in the BCP solidified/stabilized soil (see Figs. 10 and 11) leads to the continuous improvement in soil strength (see Fig. 1(a)). Meanwhile, both the time-/dosage-dependent accumulation and crystalline phase of heavy metal-bearing products result in the increased I_R value of heavy metals but decreased leachability of the solidified/stabilized soil (see Figs. 2 and 5).

4. Discussion

4.1 The contributions of CCR and PG to soil solidification/stabilization

The dominant components of carbide calcium residue (CCR) and phosphogympsum (PG) are calcium hydroxide ($Ca(OH)_2$) and gypsum ($CaSO_4 \cdot 2H_2O$), respectively (Du et al., 2016; Rashad, 2017). In this study, CCR and PG were mainly used as chemical admixtures to improve the reactivity of basic oxygen furnace slag (BOFS).

With the addition of BCP to the contaminated soil, the $Ca(OH)_2$ contained in CCR rapidly dissolve and improve the pH of the solidified/stabilized soil (see Fig. 1(b)). Then, the high pH of the solidified/stabilized soil accelerates the hydration of the silicates (i.e., C_2S and C_3S) contained in BOFS and simultaneous pozzolanic reaction occurred in the solidified/stabilized soil matrix (Poh et al., 2006; Du et al., 2014). In the hydration and pozzolanic reactions, amounts of calcium silicate hydrate (C-S-H) formed (Fig. 8). The cementation and soil pore filling effects of C-S-H contribute to the improvement in soil strength (Fig. 1(a)). Meanwhile, the absorptivity and encapsulation of C-S-H lead to the immobilization of heavy metals (Poh et al., 2006; Jiang et al., 2015).

On the other hand, the presence of gypsum ($CaSO_4 \cdot 2H_2O$) in the solidified/stabilized soil can facilitate the formation of ettringite (AFt) which has prominent mechanical property and ion-exchange capacity (Chrysochoou and Dermatas, 2006; Du et al., 2014). Hence, the soil pore filling effects of proper amount of formed AFt contributes to the improvement in soil strength (Fig. 1(a)). Meanwhile, the ion-exchange of heavy metals with AFt reduces the leached concentrations of heavy metals (Fig. 2).

In summary, the primary contributions of CCR and PG to the soil solidification/stabilization are to enhance the reactivity of BOFS which can trigger the subsequent hydration of the silicates contained in BOFS and simultaneous pozzolanic reaction in the solidified/stabilized soil matrix. With the formation of C-S-H and proper amount of AFt,

the heavy metals in the contaminated soil are immobilized and the strength of the treated soil is elevated.

4.2 Environmental impact

As hazardous or waste materials, the contaminated soils, BOFS, CCR, and PG are commonly destined for landfill disposal, which conflicts the sustainable development strategy by decreasing the efficiencies in using of landfill space, resources, and energy. Embodied energy and carbon footprint are extensively adopted indicators to evaluate the environmental sustainability of construction materials. Embodied energy and carbon footprint are defined as the total amount of energy associated and carbon emitted during the production of construction materials (Soga et al., 2011; Kua et al., 2016). These raw materials such as BOFS, CCR, and PG are not purposefully manufactured for construction materials and hence they are technically zero embodied energy and carbon footprint. On the other hand, the embodied energy and carbon footprint of PC are 4.60 MJ/kg and 0.23 kg C/kg (Hammond et al., 2008; Cagiao et al., 2011). In other words, if 1 kg of PC is substituted by 1 kg of BCP, the needed energy and emitted carbon in the stabilization/solidification of contaminated soil will be reduced by 4.60 MJ/kg and 0.23 kg C/kg, respectively. Hence, the reduced consumption of PC by opting for BCP binder would significantly reduce negative environmental impacts.

With stabilization/solidification, the contaminated soil has the potential to be reused as a construction material. However, when the solidified/stabilized soil is embedded in the soil strata, a common concern would be the ambient soil or groundwater contamination due to the leaching behavior. Fig. 12 shows a typical pavement road cross-section in which the BCP solidified/stabilized soil is used beneath the pavement layer. The black arrows in Fig. 12 represent the potential flow of precipitation across the pavement structure. In the pavement

design, most of the rainwater is expected to be surface runoff and then flow into adjacent drainage system due to the waterproof asphalt layer. Nevertheless, a small portion of naturally occurring precipitation would infiltrate into the pavement layer. The downward percolation of the precipitation would gradually carry certain amount of heavy metals across the solidified/stabilized soil filling layer into the substratum clean soil, and subsequently converge with the groundwater (red solid arrows). Furthermore, the downward and horizontal diffusion of heavy metals from the solidified/stabilized soil to ambient soil (blue arrows) is other threat to the surrounding soil environment. From the China HJ/T 299 leaching test results (Fig. 2), it is seen that with appropriate binder dosage and curing time (i.e., 8% and 28 d), the leached concentrations of heavy metals from the BCP solidified/stabilized soil can meet the criterion for groundwater quality of Class IV prescribed in China GB/T 14848 (China GAQSIQ and China SA, 2017). This leaching test, similar to USEPA Method 1312 (USEPA, 1994), is intended to simulate the leaching behavior of solid materials due to exposure to acid rain (China MEP, 2007). The substratum soil as shown in Fig. 12 can prevent direct contact between the solidified/stabilized soil and aquifer. Furthermore, the impacts of migrated heavy metals from the solidified/stabilized soil to the groundwater quality depends on not only the leached concentrations, but also the hydraulic and diffusive properties of the solidified/stabilized soil layer and substratum soil layer, the rainfall percolation rate through the pavement layer, covering soil, solidified/stabilized soil, and substratum soil (see Fig. 12), and even the hydrological conditions of the reuse scenario (Du et al., 2009; Kua et al., 2016). Therefore, further research is suggested to investigate the migration characteristics of heavy metals from on-site solidified/stabilized soil to ambient environment, such as site-specific tests, theoretical analysis based on advection-diffusion-dispersion theory, and post-implementation monitoring of field-scale remediated sites.

Table 10 shows the total and leached concentrations of heavy metals in basic oxygen furnace slag (BOFS), calcium carbide residue (CCR), and phosphogypsum (PG) tested in this study. As prescribed in China GB 36600 (China MEE and China GAQSIQ, 2018) and China GB/T 14848 (China GAQSIQ and China SA, 2018), the suggested elements of Ni, Zn, Pb, Cd, Cu, Cr, As, and Hg were evaluated in this study. It is seen Pb, Cu, and Cr in BOFS, Zn and Pb in BOFS, and Cd and Cu in PG were detected. However, no leached concentrations of these elements were detected. Hence, the BOFS, CCR, and PG used in this study are environmentally friendly materials that do not pose potential risk to environment and human health.

4. Conclusions

This study presented a systematic investigation on using a sustainable BCP binder, which was composed of basic oxygen furnace slag (BOFS) activated with mixed calcium carbide residue (CCR) and phosphogypsum (PG), to solidify/stabilize an electroplating industrial site soil contaminated with nickel (Ni) and zinc (Zn). Major conclusions can be drawn as follows:

(1) The addition of BCP binder effectively changed the geoenvironmental properties of the contaminated soil. The soil pH and unconfined compressive strength remarkably increased, but the EC and leachability of the contaminated soil significantly decreased.

(2) After BCP stabilization/solidification, the relative binding intensity index (I_R) of target heavy metals including nickel (Ni) and zinc (Zn) in soil was considerably improved. It was also verified that the I_R value of heavy metals had a good linear relationship with their leached concentrations on a semi-logarithmic scale.

(3) Binder dosage and curing time reduced the pore volume of BCP solidified/stabilized soil, resulting in the enhanced strength of the solidified/stabilized soil. Peak analysis results demonstrated that the mean diameter of the soil pores decreased with increasing binder

dosage and/or curing time.

(4) The cementation property of calcium silicate hydrate (C-S-H) and the soil pore filling effects of ettringite (AFt), portlandite, and heavy metal-bearing precipitates lead to the improvement in soil strength. The formation of $Ni(OH)_2$, Ni-Fe layered double hydroxides, $CaZn_2(OH)_6 \cdot 2H_2O$, and $Zn_5(OH)_8Cl_2 \cdot H_2O$ contributed to the enhanced binding intensity of heavy metals. Furthermore, the absorptivity of C-S-H, heavy metals encapsulation by C-S-H, and the ion-exchange of heavy metals with AFt facilitated the immobilization of heavy metals in the solidified/stabilized soil.

(5) Curing time and binder dosage had remarkable influences on the effectiveness of BCP binder within their ranges presented in this study. The time- or dosage-dependent accumulation of reaction products led to the continuous improvement in soil strength. Meanwhile, both the time- or dosage-dependent accumulation and crystalline phase of heavy metal-bearing products resulted in the decreased leached concentrations of heavy metals in the solidified/stabilized soil.

Declaration of competing interest

The authors declare that they have no known competing financial interests or personal relationships that could have appeared to influence the work reported in this paper.

CRediT authorship contribution statement

Ya-Song Feng: Conceptualization, Methodology, Investigation, Writing - Original Draft. **Yan-Jun Du:** Conceptualization, Methodology, Writing - Review & Editing, Supervision, Funding acquisition. **Annan Zhou:** Investigation, Writing - Review & Editing. **Ming Zhang:** Supervision, Writing - Review & Editing. **Jiangshan Li:** Writing - Review & Editing. **Shi-Ji Zhou:** Writing - Review & Editing. **Wei-Yi Xia:** Writing - Review & Editing.

Acknowledgments

Financial support for this project was provided by the National key R&D Program of China

(No. 2019YFC1806000), National Natural Science Foundation of China (Grant No. 41877248), Environmental Protection Scientific Research Project of Jiangsu Province (Grant No. 2016031), and Jiangsu Province Funded Project for Recruiting Postdoctoral Researchers (Grant No. 2019Z037). The first author would also acknowledge the China Scholarship Council (CSC) for supporting his study at Tohoku University and National Institute of Advanced Industrial Science and Technology (AIST), Japan.

References

Ansari, N., Seifi, A., 2013. A system dynamics model for analyzing energy consumption and CO_2 emission in Ianian cement industry under various production and export scenarios. Energy Policy, 58: 75–89. https://doi.org/10.1016/j.enpol.2013.02.042.

American Society for Testing and Materials (ASTM). ASTM D1633 Standard test methods for compressive strength of molded soil-cement cylinders. ASTM, West Conshohocken, PA, 2017.

American Society for Testing and Materials (ASTM). ASTM D4972 Standard test method for pH of soil. ASTM, West Conshohocken, PA, 2019.

Cagiao, J., Gomez, B., Domenech, J.L., Mainar, S.G., Lanza, H.G., 2011. Calculation of the corporate carbon footprint of the cement industry by the application of MC3 methodology. Ecol. Indic., 11(6): 1526–1540. https://doi.org/10.1016/j.ecolind.2011.02.013.

Cai, G.H., Liu, S.Y., Du, G.Y., Wang, L., 2019. Effect of MgO activity index on physicochemical, electrical and mechanical properties of carbonated MgO-admixed silt. KSCE J. Civ. Eng., 23(9): 3807–3817. https://doi.org/10.1007/s12205-019-0955-8.

Cai, G.H., Liu, S.Y., Zheng X., 2019. Effects of drying-wetting cycles on the durability of reactive magnesia-carbonated fine-grained soil. J. Mater. Civil Eng., 2019, 31(11): 04019276. https://doi: 10.1061/(ASCE)MT.1943-5533.0002940.

China General Administration of Quality Supervision, Inspection and Quarantine of the (China GAQSIQ) and Standardization Administration of China (China SA). GB/T 14848 Standard for groundwater quality, Beijing, 2017.

China Ministry of Ecology and Environment (China MEE). HJ/T 299 Solid waste–Extraction procedure for leaching toxicity–Sulphuric acid and nitric acid method, Beijing, 2007.

China Ministry of Ecology and Environment (China MEE). HJ 680 Solid and sedimen–Determination of mercury, arsenic, selenium, bismuth, antimony–Microwave dissolution/Atomic fluorescence spectrometry, Beijing, 2013.

China Ministry of Ecology and Environment (China MEE). HJ 766 Solid Waste–Determination of metals–Inductively coupled plasma mass spectrometry (ICP-MS), Beijing, 2015.

China Ministry of Ecology and Environment (China MEE) and China General Administration of Quality Supervision, Inspection and Quarantine (China GAQSIQ). GB 36600 Soil environmental quality–Risk control standard for soil contamination of development land, Beijing, 2018.

Constantino, V.R.L., Pinnavaia, T.J., 1995. Basic properties of $Mg_{1-x}^{2+}Al_x^{3+}$ layered double hydroxides intercalated by carbonate, hydroxide, chloride, and sulfate anions. Inorg. Chem., 34: 883–892. https://doi.org/10.1021/ic00108a020.

Chen, Z., Lu, S., Tang, M., Lin, X., Qiu, Q., He, H., Yan J., 2019. Mechanochemical stabilization of heavy metals in fly ash with additives. Sci. Total Environ., 694: 133813. https://doi.org/10.1016/j.scitotenv.2019.133813.

Davidson, C.M., Duncan, A.L., Littlejohn, D., Ure, A.M., Garden, L.M., 1998. A critical evaluation of the three-stage BCR sequential extraction procedure to assess the potential mobility and toxicity of heavy metals in industrially-contaminated land, Anal. Chim. Acta, 363(1): 45–55. https://doi.org/10.1016/S0003-2670(98)00057-9.

Dong, Q., Zhao, X., Chen, X., Ma, X., Cui, X., 2020. Long-term mechanical properties of in situ semi-rigid base materials. Road Mater. Pavement 5: 1–16. https://doi.org/10.1080/14680629.2019.1710239.

Du, Y.J., Shen, S.L., Liu, S.Y., Hayashi, S., 2009. Contaminant mitigating performance of Chinese standard municipal solid waste landfill liner systems. Geotext. Geomembranes. 27: 232–239. https://doi.org/10.1016/j.geotexmem.2008.11.007.

Du, Y.J., Jiang, N.J., Liu, S.Y., Jin, F., Singh, D.N., Puppala, A.J., 2014. Engineering properties and microstructural characteristics of cement-stabilized zinc-contaminated kaolin. Can. Geotech. J., 51(3): 289–302. https://doi.org/10.1139/cgj-2013-0177.

Du, Y.J., Jiang, N.J., Liu, S.Y., Horpibulsuk, S., Arulrajah, A., 2016. Field evaluation of soft highway subgrade soil stabilized with calcium carbide residue. Soils Found 56(2):301–314. https://doi.org/10.1016/j.sandf.2016.02.012.

Du, Y.J., Wu, J., Bo, Y.L., Jiang N.J., 2020. Effects of acid rain on physical, mechanical and chemical properties of GGBS–MgO-solidified/stabilized Pb-contaminated clayey soil. Acta Geotech., 15: 923–932. https://doi.org/10.1007/s11440-019-00793-y.

Belhadj E., Diliberto C., Lecomte A., 2012. Characterization and activation of basic oxygen furnace slag. Cement Concrete Comp., 34(1): 34-40. https://doi.org/10.1016/j.cemconcomp.2011.08.012.

Feng, Y.S., Du, Y.J, Reddy, K.R., Xia, W.Y., 2018. Performance of two novel binders to stabilize field soil with zinc and chloride: Mechanical properties, leachability and mechanisms assessment. Constr. Build. Mater., 189: 1191–1199. https://doi.org/10.1016/j.conbuildmat.2018.09.072.

Gijbels, K., Landsberger, S., Samyn, P., Iacobescu, R.I., Pontikes, Y., Schreurs, S., Schroeyers, W., 2019. Radiological and non-radiological leaching assessment of alkali-activated materials containing ground granulated blast furnace slag and phosphogypsum. Sci. Total

Environ., 660: 1098-1107. https://doi.org/10.1016/j.scitotenv.2019.01.089.

Gollakota, A.R.K., Volli, V., Shu, C.M., 2019. Progressive utilisation prospects of coal fly ash: a review. Sci. Total Environ., 672: 951-989. https://doi.org/10.1016/j.scitotenv.2019.03.337.

Gusiatin, Z.M., Kulikowska, D., 2014. The usability of the I_R, RAC and MRI indices of heavy metal distribution to assess the environmental quality of sewage sludge composts. Waste Manage., 34(7): 1227–1236. https://doi.org/10.1016/j.wasman.2014.04.005.

Hammond, G.P., Jones, C.I., 2008. Embodied energy and carbon in construction materials. Energy, 161(2): 87–98. https://doi.org/10.1680/ener.2008.161.2.87.

Han, F.X., Banin, A., Kingery, W.L., Triplett, G.B., Ding, W.X., 2003. New approach to studies of heavy metal redistribution in soil. Adv. Environ. Res., 8(1): 113–120. https://doi.org/10.1016/S1093-0191(02)00114-9.

Hasanbeigi, A., Price, L., Lin, E., 2012. Emerging energy-efficiency and CO_2 emission-reduction technologies for cement and concrete production: A technical review. Renew. Sust. Energ. Rev., 16(8): 6220–6238. https://doi.org/10.1016/j.rser.2012.07.019.

Haynes W.M., 2014. Handbook of chemistry and physics. CRC press, Boca Raton.

Horpibulsuk, S., Rachan, R., Raksachon, Y., 2009. Role of fly ash on strength and microstructure development in blended cement stabilized silty clay. Soils Found., 2009, 49(1): 85–98. https://doi.org/10.3208/sandf.49.85.

Hua, Y., Heal, K.V., Friesl-Hanl, W., 2017. The use of red mud as an immobiliser for metal/metalloid-contaminated soil: A review. J. Hazard. Mater., 325: 17–30. https://doi.org/10.1016/j.jhazmat.2016.11.073

Japanese Geotechnical Society (JGS). 0212 Test method for electrical conductivity of soils, JGS, Tokyo, 2010.

Jiang, N.J., Du, Y.J., Liu, S.Y., Wei, M.L., Horpibulsuk, S., Arulrajah, A., 2015. Multi-scale

laboratory evaluation of the physical, mechanical, and microstructural properties of soft highway subgrade soil stabilized with calcium carbide residue. Can. Geotech. J., 53(3): 373–383. https://doi.org/10.1139/cgj-2015-0245.

Jiang, N.J., Du, Y.J., Liu, K., 2018. Durability of lightweight alkali-activated ground granulated blast furnace slag (GGBS) stabilized clayey soils subjected to sulfate attack. Appl. Clay Sci., 161: 70-75. https://doi.org/10.1016/j.clay.2018.04.014.

Johnson, C.A., Glasser, F.P., 2003. Hydrotalcite-like minerals ($M_2Al(OH)_5(CO_3)_{0.5}\cdot H_2O$, where M=Mg, Zn, Co, Ni) in the environment: Synthesis, characterization and thermodynamic stability. Clay. Clay Miner., 51: 1–8. https://doi.org/10.1346/CCMN.2003.510101.

Khoshghalb, A., Pasha, A.Y., Khalili, N., 2015. A fractal model for volume change dependency of the water retention curve. Géotechnique, 65(2): 141–146. https://doi.org/10.1680/geot.14.T.016.

Krehula, S., Ristić, M., Wu, C., Li, X., Jiang, L., Wang, J., Sun, G., Zhang, T., Perović, M., Bošković, M., Antić, B., Kratofil Krehula, L., Kobzi, B., Kubuki, S., Musić, S., 2018. Influence of Fe (III) doping on the crystal structure and properties of hydrothermally prepared β-Ni(OH)$_2$ nanostructures. J. Alloy. Compd., 750: 687–695. https://doi.org/10.1016/j.jallcom.2018.04.032.

Kua, T.A., Arulrajah, A., Horpibulsuk, S., Du, Y.J., Suksiripattanapong, C., 2016. Engineering and environmental evaluation of spent coffee grounds stabilized with industrial by-products as a road subgrade material. Clean Technol. Envir., 19(1), 1–13. https://doi.org/10.1007/s10098-016-1188-x.

Kurda, R., Silvestre, J.D., de Brito, J., 2018. Life cycle assessment of concrete made with high volume of recycled concrete aggregates and fly ash. Resour. Conserv. Recy., 139: 407–417. https://doi.org/10.1016/j.resconrec.2018.07.004.

Li, X., Zhang, L.M., 2009. Characterization of dual-structure pore-size distribution of soil. Can. Geotech. J., 46(2): 129–141. https://doi.org/10.1139/T08-110.

Li, K.W., Kumada, N., Yonesaki, Y., Takei, T., Kinomurab, N., Wang, H., Wang, C., 2010. The pH effects on the formation of Ni/Al nitrate form layered double hydroxides (LDHs) by chemical precipitation and hydrothermal method. Mater. Chem. Phys., 121(1–2): 223–229. https://doi.org/10.1016/j.matchemphys.2010.01.026.

Li, M., Zhang M., Du, C., Chen, Y., 2020. Study on the spatial spillover effects of cement production on air pollution in China. Sci. Total Environ., 748: 141421. https://doi.org/10.1016/j.scitotenv.2020.141421.

Ma, T., Wang, H., He, L., Zhao, Y., Huang, X., Chen, J., 2017. Property characterization of asphalt binders and mixtures modified by different crumb rubbers. J. Mater. Civil Eng., 29(7): 04017036. https://doi.org/10.1061/(ASCE)MT.1943-5533.0001890.

Mikulčić, H, Cabezas, H, Vujanović, M, Duić, N., 2016. Environmental assessment of different cement manufacturing processes based on Emergy and Ecological Footprint analysis. J. Clean. Prod., 130: 213–221. https://doi.org/10.1016/j.jclepro.2016.01.087.

Mitchell, J.K., Soga, K., 2005. Fundamentals of Soil Behavior. Three ed. John Wiley & Sons, New York.

Oprkal, P., Mladenovi, A., Zupani, N., Anar, J., Serjun, V.Z., 2020. Remediation of contaminated soil by red mud and paper ash. J. Clean. Prod., 256: 120440. https://doi.org/10.1016/j.jclepro.2020.120440.

Oualmakran, M., Mercatoris, B., Francois, B., 2016. Pore-size distribution of a compacted silty soil after compaction, saturation, and loading. Can. Geotech. J., 53(12): 1902–1909. https://doi.org/10.1139/cgj-2016-0184.

Phummiphan, I., Horpibulsuk, S., Rachan, R., Arulrajah, A., Shen, S., Chindaprasirt, P., 2018. High calcium fly ash geopolymer stabilized lateritic soil and granulated blast furnace

slag blends as a pavement base material. J. Hazard. Mater., 341: 257–267. https://doi.org/10.1016/j.jhazmat.2017.07.067.

Poh, H.Y., Ghataora, G.S., Ghazireh, N., 2006. Soil stabilization using basic oxygen steel slag fines. J. Mater. Civil. Eng., 18(2): 229–240. https://doi.org/10.1061/(ASCE)0899-1561(2006)18:2(229).

Proctor, D.M., Fehling, K.A., Shay, E.C., Wittenborn, J.L., Green, J.J., Avent, C., Bigham, R.D., Connolly, M., Lee, B., Shepker, T.O., Zak M.A., 2000. Physical and chemical characteristics of blast furnace, basic oxygen furnace, and electric arc furnace steel industry slags. Environ. Sci. Technol., 34(8): 1576–1582. https://doi.org/10.1021/es9906002.

Rahman, M.A., Imteaz, M.A., Arulrajah, A., Piratheepan, J., Disfani, M.M., 2015. Recycled construction and demolition materials in permeable pavement systems: geotechnical and hydraulic characteristics. J. Clean. Prod., 90: 183–194. https://doi.org/10.1016/j.jclepro.2014.11.042.

Rashad, A.M., 2017. Phosphogypsum as a construction material. J. Clean. Prod., 166: 732–743. https://doi.org/10.1016/j.jclepro.2017.08.049.

Sharma, H.D., Reddy K.R., 2004. Geoenvironmental engineering: site remediation, waste containment, and emerging waste management technologies, John Wiley & Sons, New York.

Shi, C., 2004. Steel slag–Its production, processing, characteristics and cementitious properties. J. Mater. Civil. Eng., 16(3): 230–236. https://doi.org/10.1061/(ASCE)0899-1561(2004)16:3(230).

Simms, P.H., Yanful, E.K., 2001. Measurement and estimation of pore shrinkage and pore distribution in a clayey till during soil-water characteristic curve tests. Can. Geotech. J., 38(4): 741–754. https://doi.org/10.1139/t01-014.

Soga, K., Chau, C., Nicholson, D., Pantelidou, H. 2011. Embodied energy: soil retaining geosystems. KSCE J. Civ. Eng., 15(4): 739–749. https://doi.org/10.1007/s12205-011-0013-7.

Spence, R.D., Shi, C., 2004. Stabilization and Solidification of Hazardous, Radioactive, and Mixed Wastes, CRC Press, Boca Raton.

Srivastava, O.K., Secco, E.A., 2011. Studies on metal hydroxy compounds. II. Infrared spectra of zinc derivatives ε-$Zn(OH)_2$, β-ZnOHCl, ZnOHF, $Zn_5(OH)_8Cl_2$, and $Zn_5(OH)_8Cl_2 \cdot H_2O$. Can. J. Chem., 45(6): 585–588. https://doi.org/10.1139/v67-097.

Tian, Q., Nakama, S., Sasaki, K., 2019. Immobilization of cesium in fly ash-silica fume based geopolymers with different Si/Al molar ratios. Sci. Total Environ., 687: 1127-1137. https://doi.org/10.1016/j.scitotenv.2019.06.095

US Environmental Protection Agency (US EPA), 1996. Prohibition on the disposal of bulk liquid hazardous waste in landfills-statutory interpretive guidance, US EPA, Washington DC.

US Environmental Protection Agency (US EPA), 1994. Method 1312 Synthetic Precipitation Leaching Procedure (SPLP). US EPA, Washington DC.

Vespa, M., Dähn, R., Gallucci, E., Grolimund, D., Wieland, E., Scheidegger, A.M., 2006. Microscale investigations of Ni uptake by cement using a combination of scanning electron microscopy and synchrotron-based techniques. Environ. Sci. Technol., 40(24): 7702–7709. https://doi.org/10.1021/es060957n.

Vespa, M., Wieland, E., Dähn, R., Grolimund, D., Scheidegger, A.M., 2007. Determination of the elemental distribution and chemical speciation in highly heterogeneous cementitious materials using synchrotron-based micro-spectroscopic techniques. Cement Concrete. Res., 37(11): 1473–1482. https://doi.org/10.1016/j.cemconres.2007.08.007.

Wang, S., Gao, B., Li, Y., Zimmerman, A.R., Cao, X., 2016. Sorption of arsenic onto Ni/Fe

layered double hydroxide (LDH)-biochar composites. RSC Adv., 6(22): 17792–17799. https://doi.org/10.1039/C5RA17490b.

Wu, H.L., Jin, F., Bo, Y.L., Du, Y.J., Zheng, J.X., 2018. Leaching and microstructural properties of lead contaminated kaolin stabilized by GGBS-MgO in semi-dynamic leaching tests. Constr. Build. Mater., 172: 626–634. https://doi.org/10.1016/j.conbuildmat.2018.03.164.

Wu, H.L., Du, Y.J., Yu, J., Yang, Y.L., Li, V.C., 2020. Hydraulic conductivity and self-healing performance of Engineered Cementitious Composites exposed to Acid Mine Drainage. Sci. Total Environ., 716: 137095. https://doi.org/10.1016/j.scitotenv.2020.137095.

Xia, W.Y., Feng, Y.S., Jin, F., Zhang, L.M., Du, Y.J., 2017. Stabilization and solidification of a heavy metal contaminated site soil using a hydroxyapatite based binder. Constr. Build. Mater., 156: 199–207. https://doi.org/10.1016/j.conbuildmat.2017.08.149.

Xia, W.Y., Du, Y.J., Li, F.S., Li, C.P., Yan, X.L., Arulrajah, A., Wang F., Song, D.J., 2019. In-situ solidification/stabilization of heavy metals contaminated site soil using a dry jet mixing method and new hydroxyapatite based binder. J. Hazard. Mater., 369: 353–361. https://doi.org/10.1016/j.jhazmat.2019.02.031.

Yang, Y.L., Reddy, K.R., Du, Y.J., Fan, R.D., 2018. Short-term hydraulic conductivity and consolidation properties of soil-bentonite backfills exposed to CCR-impacted groundwater. J. Geotech. Geoenviron. Eng., 144(6): 04018025. https://doi.org/10.1061/(ASCE)GT.1943-5606.0001877.

Zhang, T.S., Yu, Q.J., Wei, J.X., Li, J.X., Zhang, P.P., 2011. Preparation of high performance blended cement and reclamation of iron concentrate from basic oxygen furnace steel slag. Resour. Conserv. Recy., 56(1): 48–55. https://doi.org/10.1016/j.resconrec.2011.09.003.

Zhang W.J., Lin M.F., 2020. Influence of redox potential on leaching behavior of a solidified chromium contaminated soil. Sci. Total Environ., 733: 139410.

https://doi.org/10.1016/j.scitotenv.2020.139410.

Zhou, Y., Liu, Y., 2018. China's fight against soil pollution. Science, 362(6412): 298. https://doi.org/10.1126/science.aav4061.

Table 1 Basic physicochemical properties of untreated contaminated soil.

Test parameter	Value [b]	Test method
Specific gravity, G_s	2.75	ASTM D854-14
Liquid limit, w_L (%)	37.2	ASTM D4318-10
Plastic limit, w_P (%)	18.1	ASTM D4318-10
Optimum water content, w_{opt} (%)	18.7	ASTM D698-12
Maximum dry density, ρ_d (g/cm^3)	1.68	ASTM D698-12
Soil pH	5.82	ASTM D4972-18
Soil classification	CL	ASTM D2487-17
Grain size distribution (%) [a]		—
Clay (<0.002 mm)	22.1	
Silt (0.002-0.075 mm)	70.3	
Sand (0.075-20 mm)	7.6	
Contaminants concentration (mg/kg)		—
Nickel, Ni	6053	HJ 766-2015
Zinc, Zn	5352	HJ 766-2015
Iron in trivalence, Fe	7515	HJ 766-2015
Chloride, Cl^-	3755	GB/T 50123-2019
Sulfate, SO_4^{2+}	1630	GB/T 50123-2019

[a] Measured using a laser particle size analyzer Mastersizer 2000 (Malvern, USA).
[b] Number of replicates = 3, and the coefficient of variance (COV) < 3.1%.

Table 2 Basic physicochemical properties of BOFS, CCR, and PG.

Test parameter	Value (%) [b]			Test method
	BOFS	CCR	PG	
Specific gravity, G_s	3.35	2.17	2.63	ASTM D854-14
pH	11.03	12.57	4.31	ASTM D4972-18
Specific surface areas (m^2/kg)	307	1263	558	China GB/T 8074-2008
Grain size distribution (%) [a]				—
<0.002 mm	16.55	19.07	9.14	
0.002-0.075 mm	79.42	73.22	71.16	
0.075-20 mm	4.03	7.71	19.7	

[a] Measured using a laser particle size analyzer Mastersizer 2000 (Malvern, USA).
[b] Number of replicates = 3, and the coefficient of variance (COV) < 2.6%.

Table 3 Chemical compositions of untreated contaminated soil, BOFS, CCR, and PG.

Oxide [a]	Weight percent (%) [c]			
	Soil	BOFS	CCR	PG
Calcium oxide (CaO)	1.93	39.59	68.02	26.13
Silicon oxide (SiO_2)	63.51	13.78	1.73	6.59
Aluminum oxide (Al_2O_3)	16.13	4.67	1.97	2.73
Phosphorus oxide (P_2O_5)	0.03	1.67	0.43	3.34
Sulphate oxide (SO_3)	0.57	0.72	1.79	33.71
Ferric oxide (Fe_2O_3)	4.82	15.97	0.37	ND [d]
Magnesium oxide (MgO)	2.17	9.53	0.22	3.57
Potassium oxide (K_2O)	2.43	0.29	ND [d]	1.51
Loss on ignition [b]	4.89	5.03	22.56	19.32

[a] Analyzed using ARL 9800 XP+XRF spectrometry.
[b] Value of loss on ignition is referenced to 950 °C.
[c] Number of replicate = 1.
[d] Not detectable.

Table 4 Binder dosage and curing time for various tests.

Test type	Binder dosage (%)	Curing time (d)	Number of replicate
UCS	4, 6, 8, 10	3, 7, 14, 28, 60, 90	3
Soil pH	4, 6, 8, 10	3, 7, 14, 28, 60, 90	3
Soil EC	4, 6, 8, 10	3, 7, 14, 28, 60, 90	3
Leaching toxicity	4, 6, 8, 10	3, 7, 14, 28, 60, 90	3
BCR SEP	4, 6, 8, 10[a]	7, 28, 60, 90[b]	1
MIP	4, 6, 8, 10[a]	7, 28, 90[b]	1
XRD	Paste, 8, 20, 50[a]	7, 28, 90[b]	1
EDS-mapping	Paste	28	1

[a] Curing time is 28 d.
[b] Binder dosage is 8%.

Table 5 Binder paste samples for XRD and SEM-EDS analysis.

Mixing denotation	Binder	Contaminant [a]	Contaminant concentration (%) [b]	Binder-solution ratio (g:ml) [c]
BCP [d]	BCP	-	-	1:0.8
BCP+Ni+Zn [d]	BCP	Ni and Zn	7.6 and 6.7	1:0.8
BCP+Ni+Zn+Fe [d]	BCP	Ni, Zn, and Fe	7.6, 6.7 and 9.4	1:0.8
BCP+Ni+Zn+Fe+SO_4^{2+}+Cl^- [e]	BCP	Ni, Zn, Fe, SO_4^{2+}, and Cl^-	3.5, 6.7, 9.4, 4.7 and 2.0	1:0.8

[a] Prepared by dissolving metals in nitrates or anions in sodium in distilled water.
[b] The percentage of the contaminant to the binder on dry weight basis.
[c] The ratio of binder weight (g) to solution volume (ml).
[d] The paste sample is subjected to XRD analysis.
[e] The paste sample is subjected to XRD, SEM, and EDS-mapping analysis.

Table 6 Variations in pore volumes of solidified/stabilized soil with curing time and binder dosage.

Dosage (%)	Curing time (d)	Total pore volume (mL/g)	Pore volume (mL/g) [a]		
			<0.01 μm	0.01-10 μm	>10 μm
8	7	0.250	0.008	0.231	0.011
8	28	0.214	0.005	0.200	0.009
8	90	0.191	0.006	0.180	0.005
4	28	0.255	0.011	0.225	0.019
6	28	0.230	0.006	0.215	0.009
8	28	0.214	0.005	0.200	0.009
10	28	0.183	0.005	0.176	0.002

[a] Number of replicate = 1.

Table 7 Parameters obtained from the peak analysis of PSD curve of solidified/stabilized soils

with different binder dosages and curing times.

Dosage (%)	Curing time (d)	n [a]	A_1 (mL/g) [b]	μ_1 [c]	σ_1 [d]	A_2 (mL/g) [b]	μ_2 [c]	σ_2 [d]	R^2 [e]
8	7	2	0.192	-0.633	0.821	0.045	-0.287	0.258	0.96
8	28	2	0.185	-0.652	0.973	0.026	-0.582	0.232	0.96
8	90	1	0.182	-0.738	1.035	—	—	—	0.93
4	28	2	0.201	-0.151	0.532	0.071	0.892	0.643	0.95
6	28	2	0.191	-0.409	0.701	0.042	0.227	0.302	0.99
8	28	2	0.185	-0.652	0.973	0.026	0.203	0.232	0.96
10	28	1	0.18	-0.916	0.916	—	—	—	0.95

[a] Number of peaks in the fitted PSD curves.
[b] A_1 and A_2, volumes of soil pores covered by simulated $f_1(d)$ and $f_2(d)$ curves.
[c] μ_1 and μ_2, logarithm of the mean diameter of soil pores fitted by $f_1(d)$ and $f_2(d)$ curves.
[d] σ_1 and σ_2, standard deviations.
[e] R^2, correlation coefficient.

Table 8 Intensity of major reaction products in solidified/stabilized soils with different curing times obtained from X-ray diffraction analysis.

Reaction products	Bragg angle (°)	Intensity (counts)		
		7 d [a]	28 d [a]	90 d [a]
Aft	9.10	837	1039	1093
	15.80	507	598	624
C-S-H	29.36	853	1110	1227
	32.02	459	493	526
Portlandite	18.10	403	472	492
	34.08	401	485	608
α-Ni(OH)$_2$	11.36	652	531	ND [b]
	22.74	ND [b]	ND [b]	ND [b]
β-Ni(OH)$_2$	19.26	551	569	489
	38.46	ND [b]	ND [b]	ND [b]
Ni-Fe LDHs (S)	10.02	ND [b]	681	ND [b]
	20.04	ND [b]	478	ND [b]
Ni-Fe LDHs (C)	11.64	ND [b]	ND [b]	634
	23.40	ND [b]	ND [b]	485
$Zn_5(OH)_8Cl_2 \cdot H_2O$	18.92	ND [b]	528	554
	38.28	ND [b]	ND [b]	ND [b]
$CaZn_2(OH)_6 \cdot 2H_2O$	14.18	483	496	479
	28.56	463	454	416

[a] Binder dosage is 8%.
[b] No peak is detected.

Table 9 Intensity of major reaction products in solidified/stabilized soils with different binder dosages obtained from X-ray diffraction analysis.

Reaction products	Bragg angle (°)	Intensity (counts)		
		8% [a]	20% [a]	50% [a]
Aft	9.10	1039	1194	1471
	15.80	598	719	794
C-S-H	29.36	1110	1327	1592
	32.02	493	547	634
Portlandite	18.10	472	488	494
	34.08	487	552	649
α-$Ni(OH)_2$	11.36	531	553	629
	22.74	ND [b]	ND [b]	463
β-$Ni(OH)_2$	19.26	551	569	617
	38.46	ND [b]	ND [b]	373
Ni-Fe LDHs (S)	10.02	681	703	771
	20.04	478	491	523
Ni-Fe LDHs (C)	11.64	ND [b]	ND [b]	759
	23.40	ND [b]	ND [b]	493
$Zn_5(OH)_8Cl_2 \cdot H_2O$	18.92	528	565	637
	38.28	ND [b]	ND [b]	ND [b]
$CaZn_2(OH)_6 \cdot 2H_2O$	14.18	496	567	603
	28.56	454	511	534

[a] Curing time is 28 d.
[b] No peak is detected.

Table 10 Total and leached concentrations of heavy metals in BOFS, CCR, and PG.

Heavy metal [a]	Total concentration (mg/kg)			Leached concentration (mg/L)		
	BOFS	CCR	PG	BOFS	CCR	PG
Nickel (Ni) [b]	<1.9 [d]	<1.9	<1.9	<0.002 [e]	<0.002	<0.002
Zinc (Zn) [b]	<3.2	7.11	<3.2	<0.5	<0.5	<0.5
Lead (Pb) [b]	1.2	0.2	<0.1	<0.005	<0.005	<0.005
Cadmium (Cd) [b]	<0.05	<0.05	0.06	<0.001	<0.001	<0.001
Copper (Cu) [b]	2.7	<1.2	6.2	<0.05	<0.05	<0.05
Chromium (Cr) [b]	0.3	<0.1	<0.1	<0.01	<0.01	<0.01
Arsenic (As) [b]	<0.5	<0.5	<0.5	<0.001	<0.001	<0.001
Mercury (Hg) [c]	<0.05	<0.05	<0.05	<0.0001	<0.0001	<0.0001

[a] The suggested elements prescribed as per China GB 36600 and China GB/T 14848.
[b] Tested as per China HJ 766 (China MEE, 2015).
[c] Tested as per China HJ 680 (China MEE, 2013).
[d] Symbol < *x* in total concentration means lower than the detection limit (*x* mg/kg).
[e] Symbol < *y* in leached concentration means lower than the detection limit (*y* mg/L).

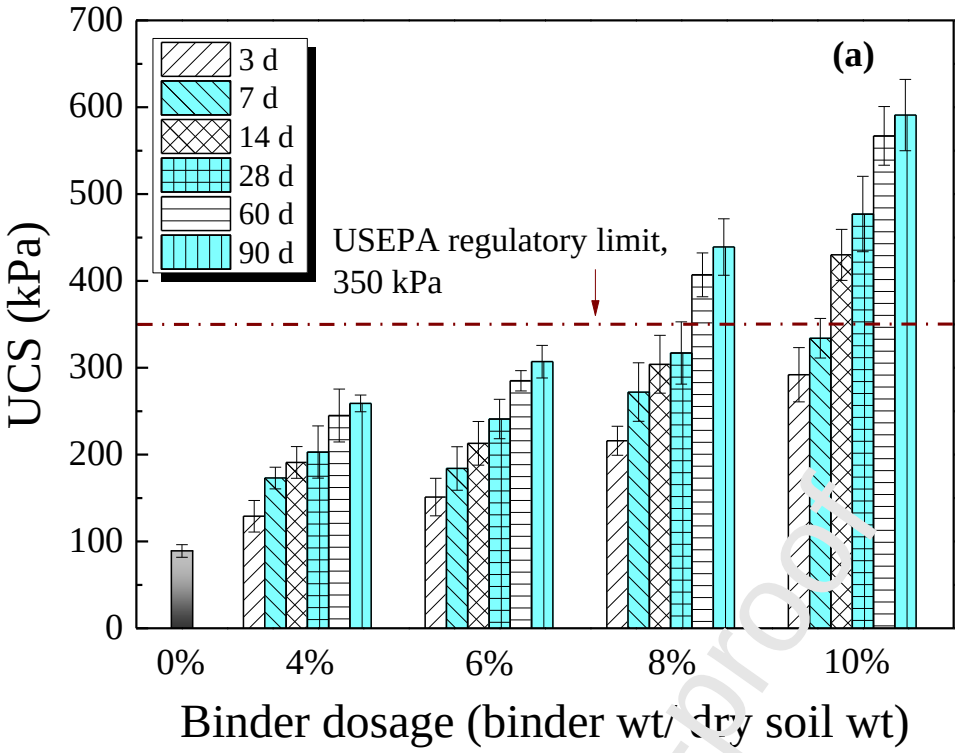

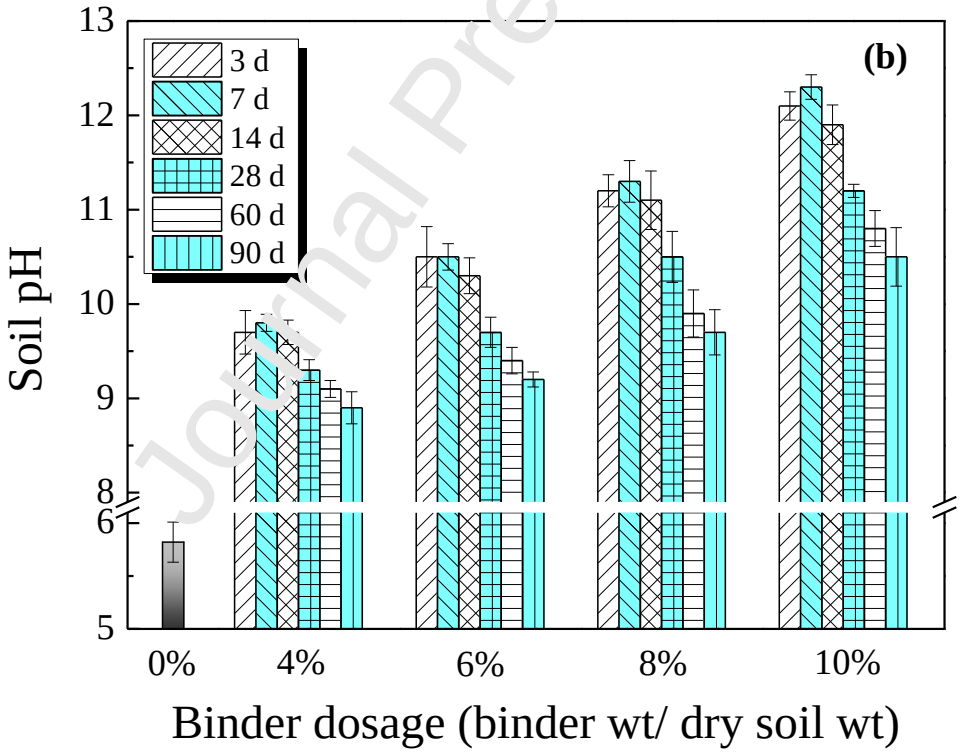

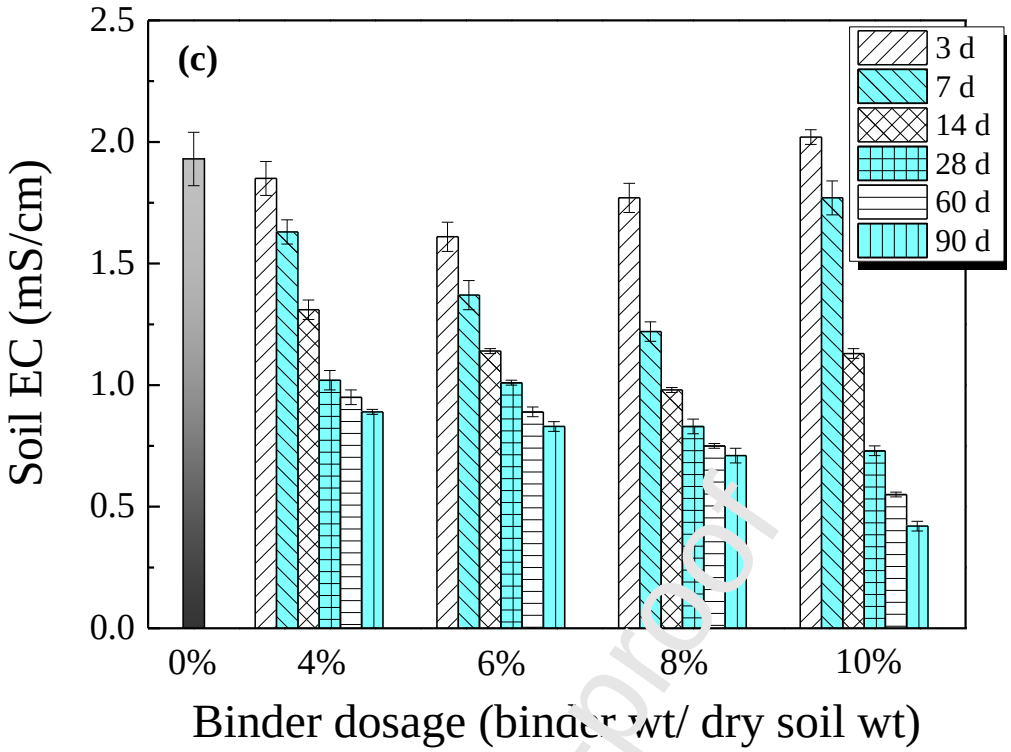

Fig. 1 Variations of soil UCS, pH, and EC with curing time and binder dosage (Number of replicates = 3, COV < 4.1%).

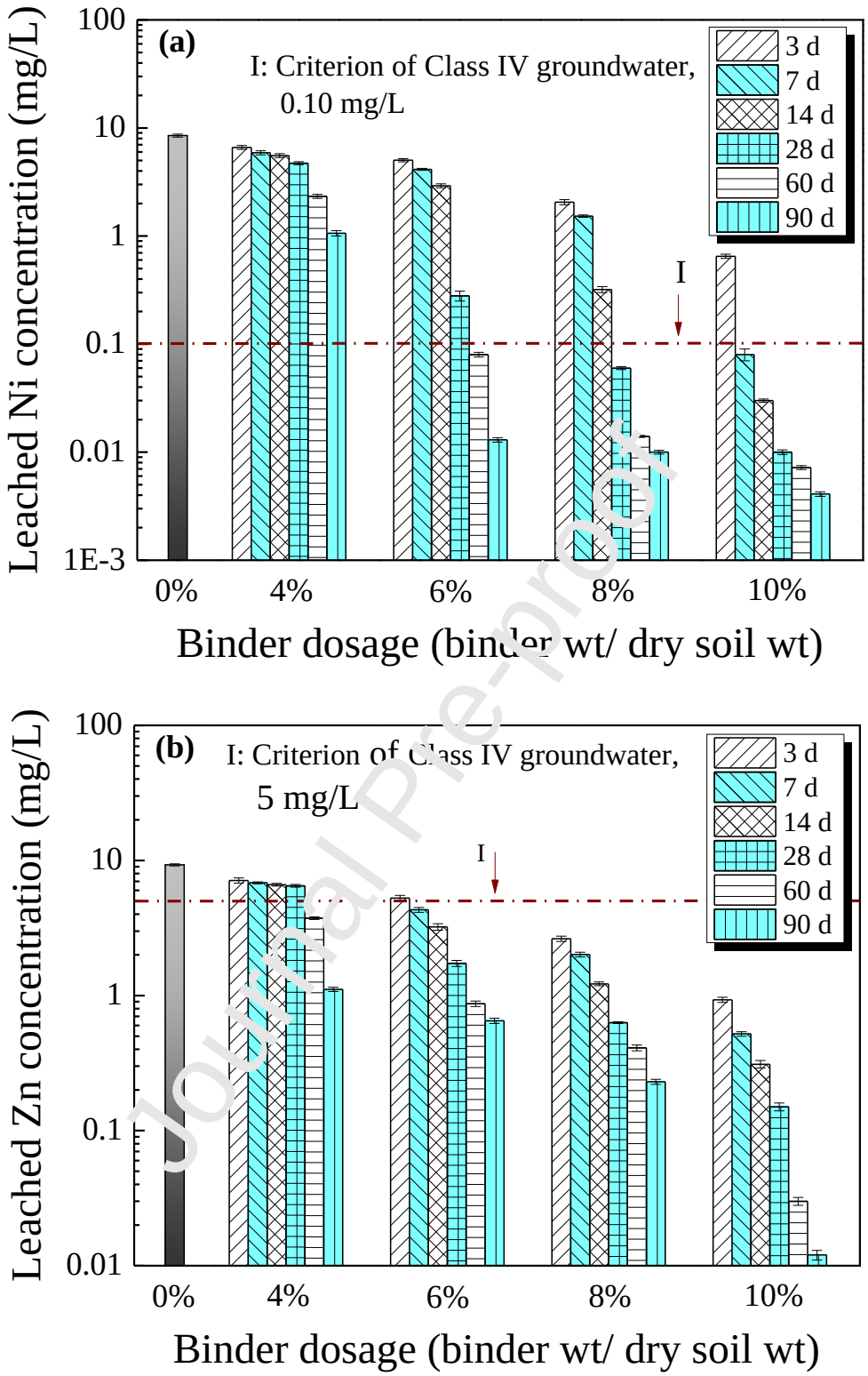

Fig. 2 Variations of the concentrations of heavy metals leached from solidified/stabilized soil with curing time and binder dosage: (a) Ni and (b) Zn (Number of replicates = 3, COV < 1.9%).

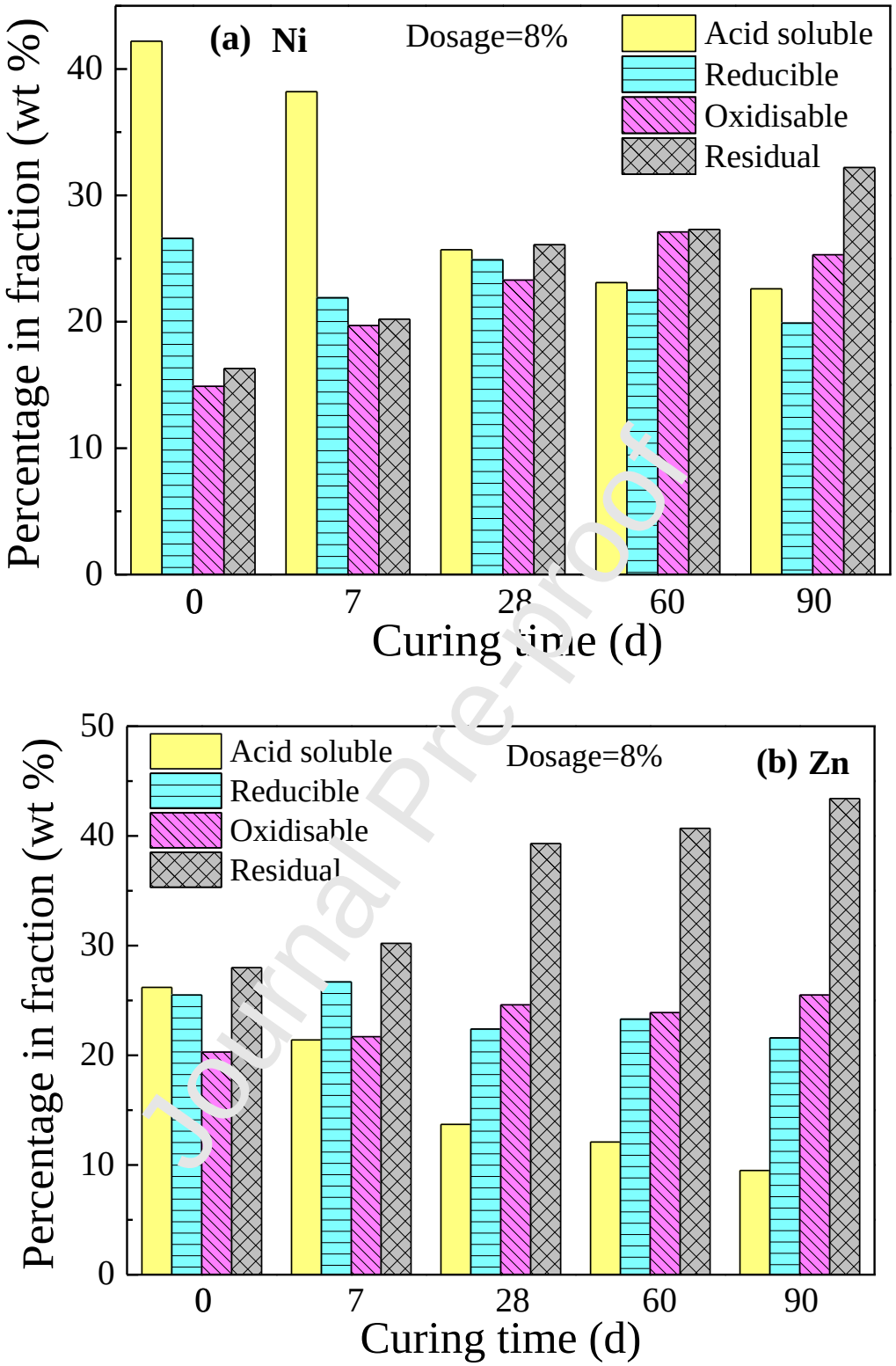

Fig. 3 Variation of chemical speciation of heavy metals contained in 8% BCP solidified/stabilized soil with curing time: (a) Ni and (b) Zn (Number of replicate = 1).

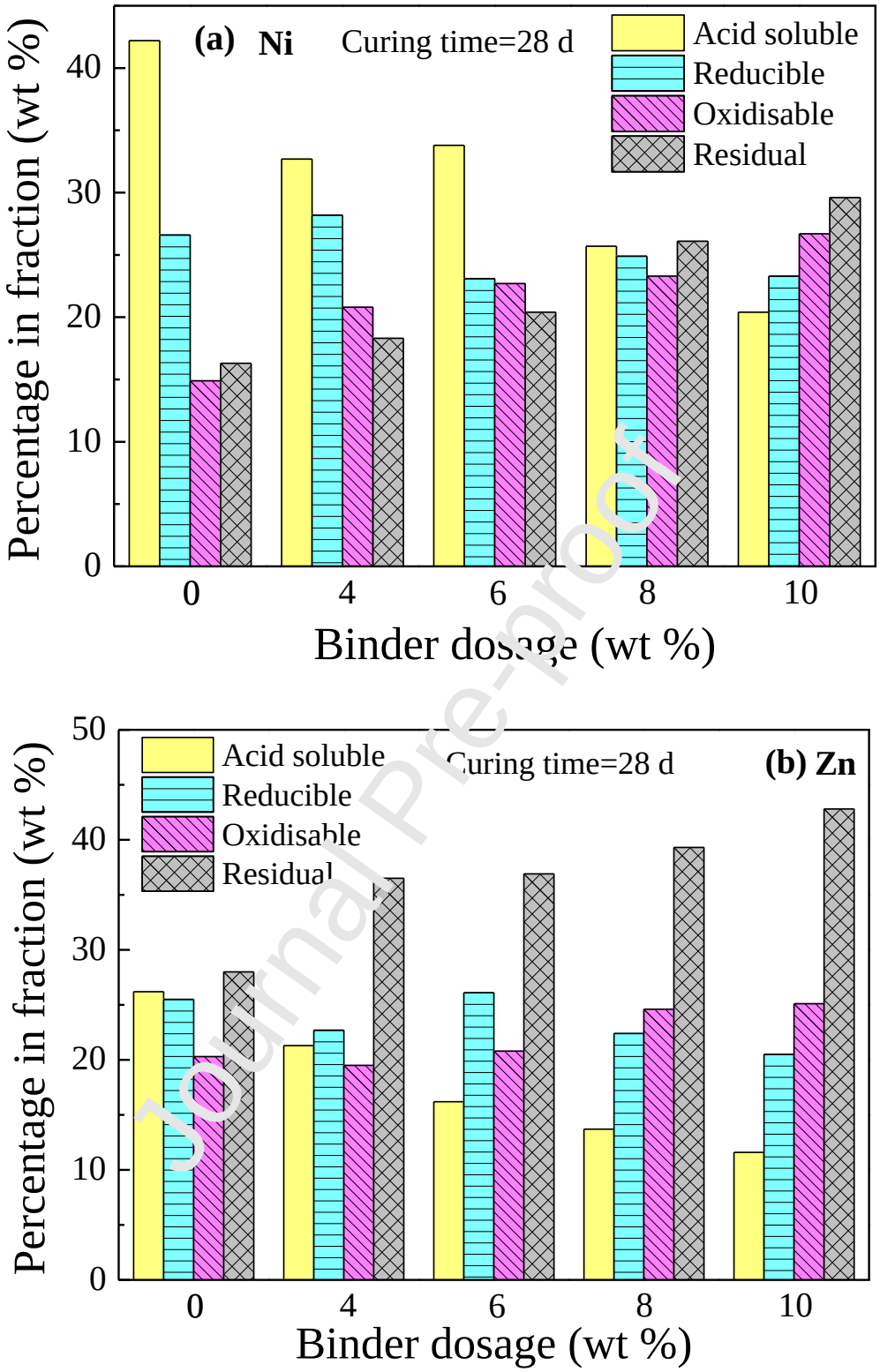

Fig. 4 Variation of chemical speciation of heavy metals contained in solidified/stabilized soil after 28 d curing with binder dosage: (a) Ni and (b) Zn (Number of replicate = 1).

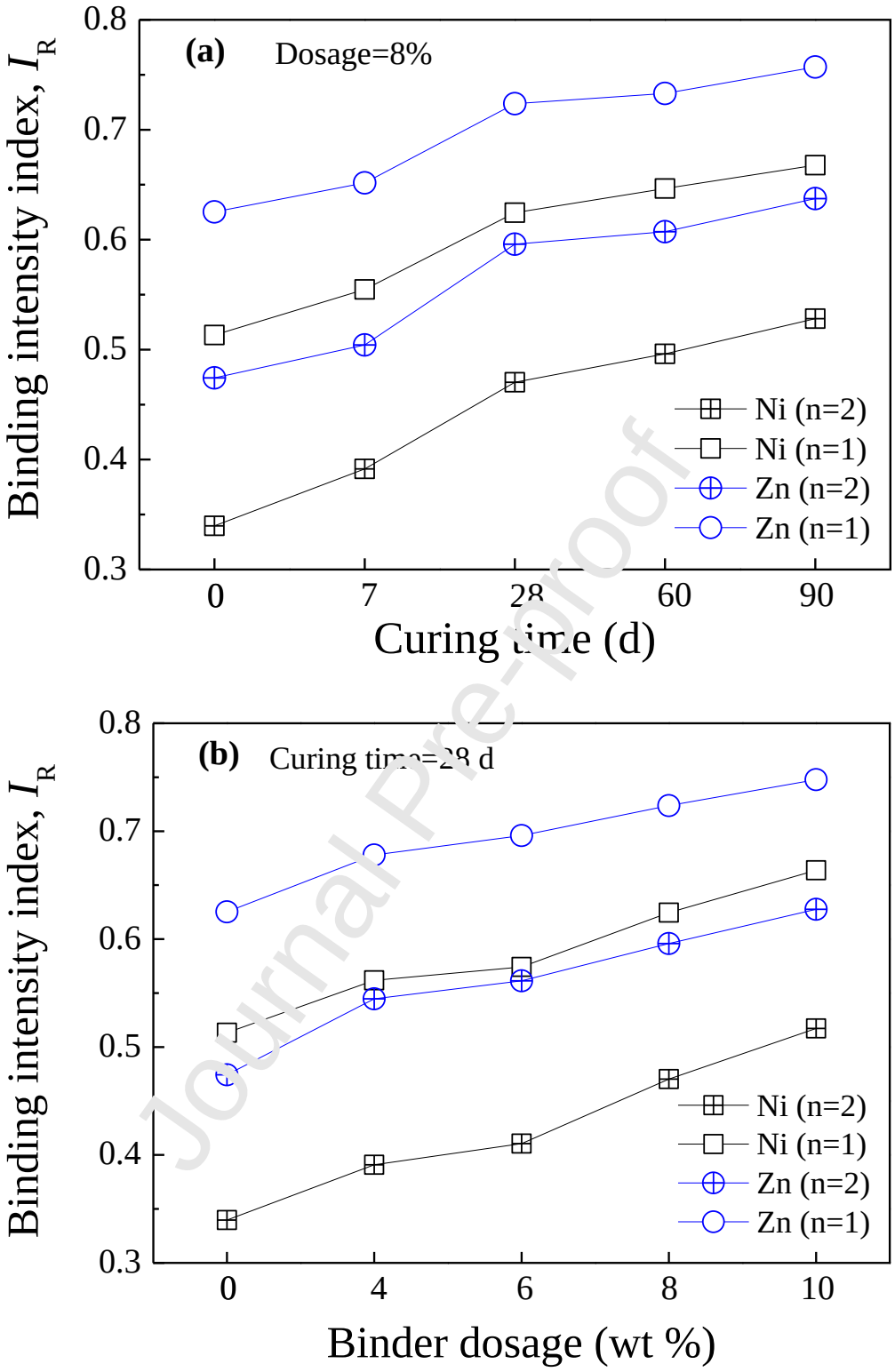

Fig. 5 Variation of relative binding intensity index (I_R) of heavy metals contained in solidified/stabilized soil with (a) curing time and (b) binder dosage (Number of replicate = 1).

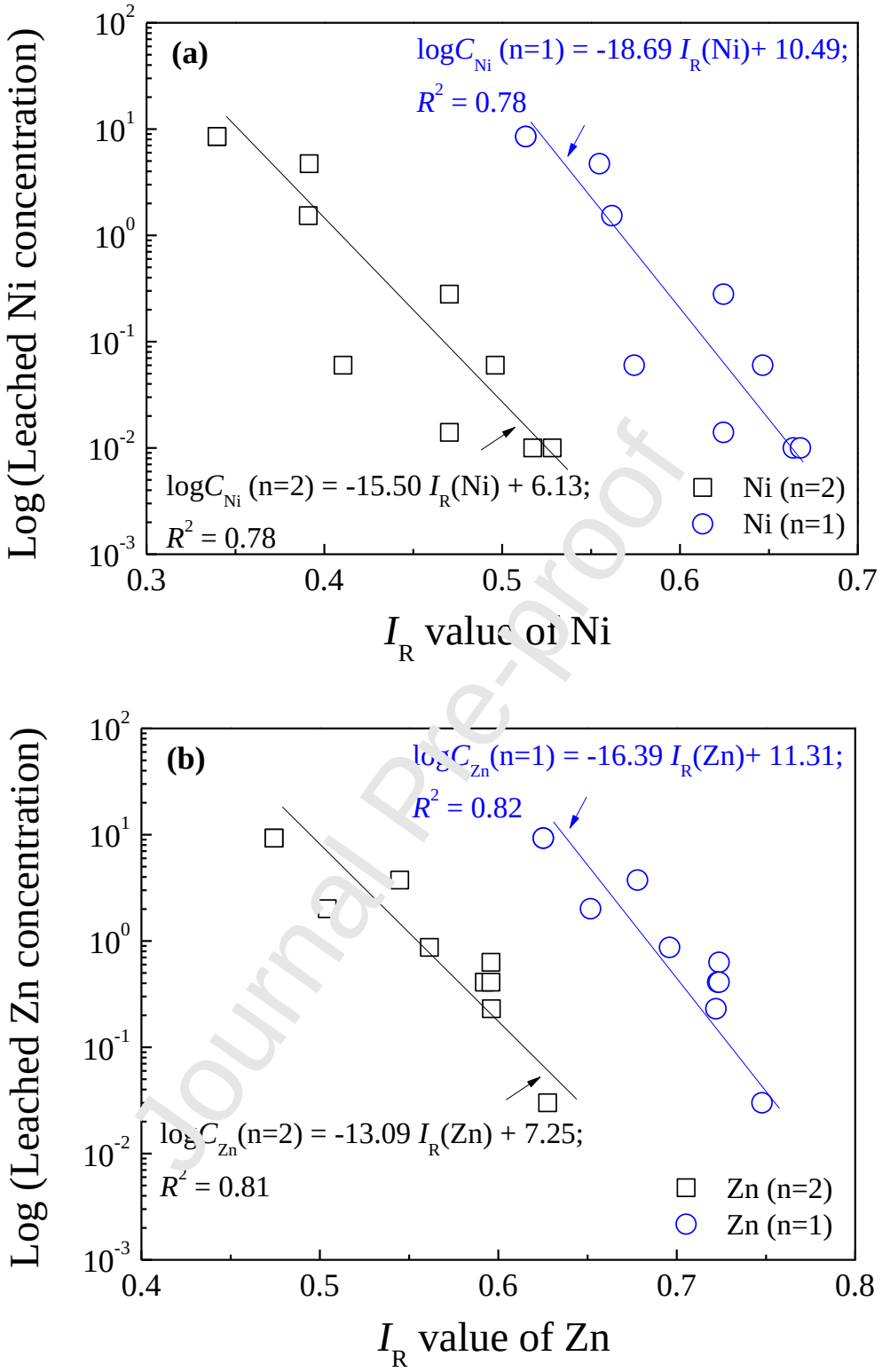

Fig. 6 Relationship between I_R and leached concentrations of heavy metals: (a) Ni, and (b) Zn.

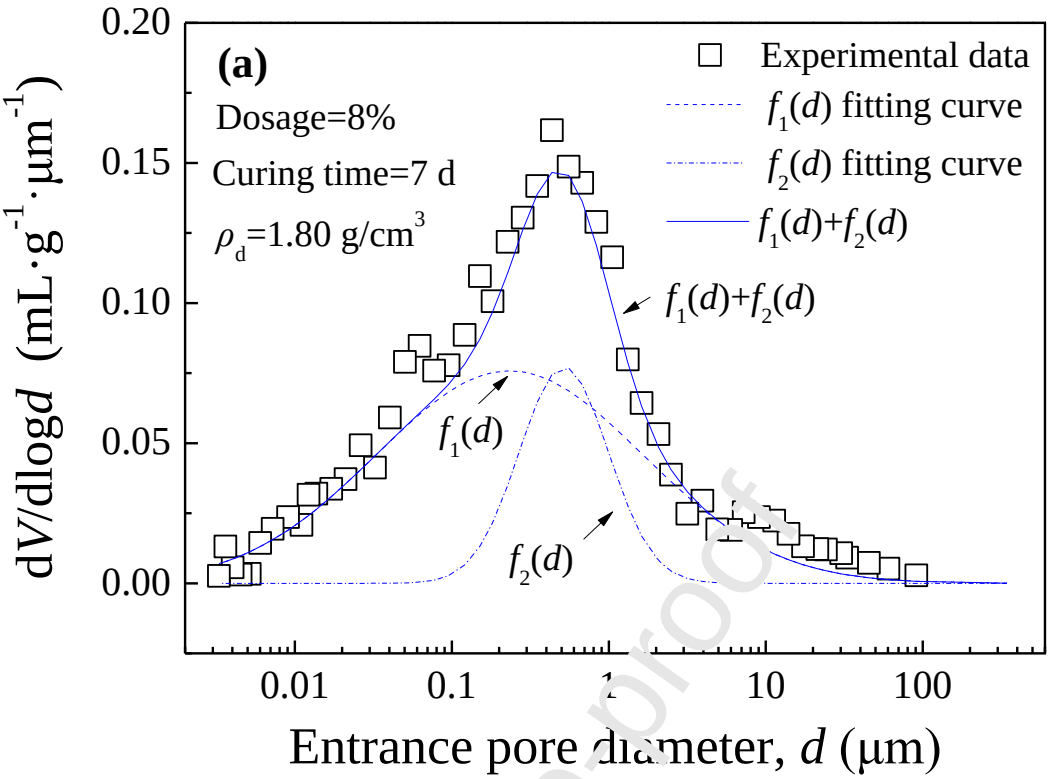

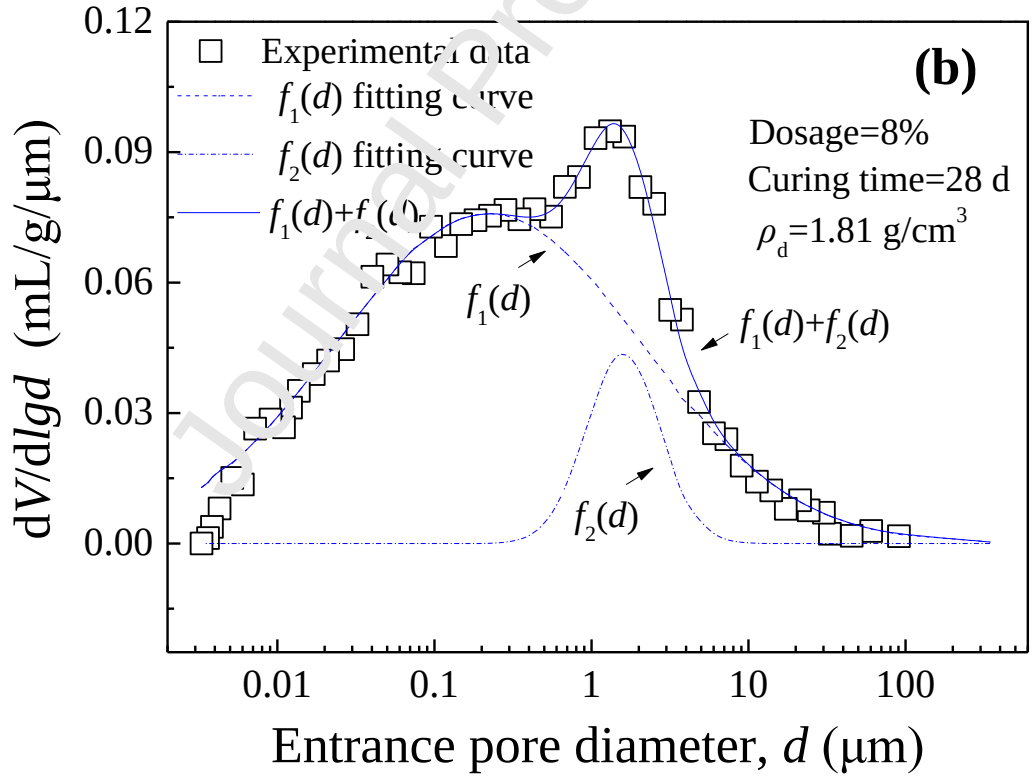

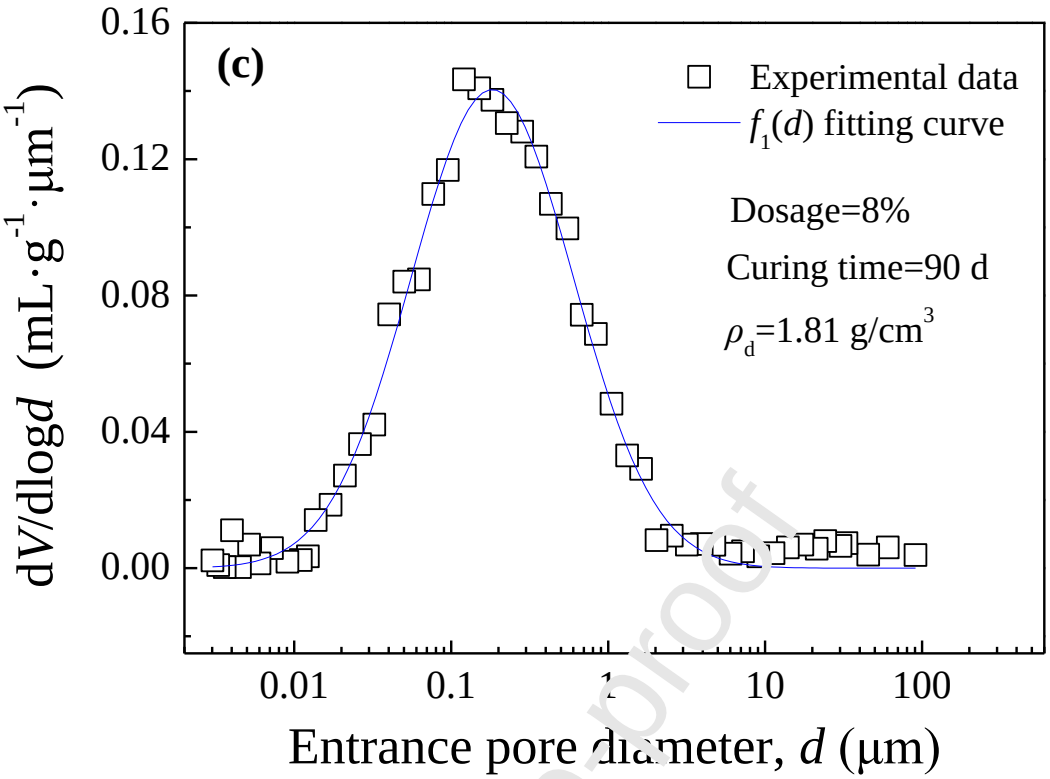

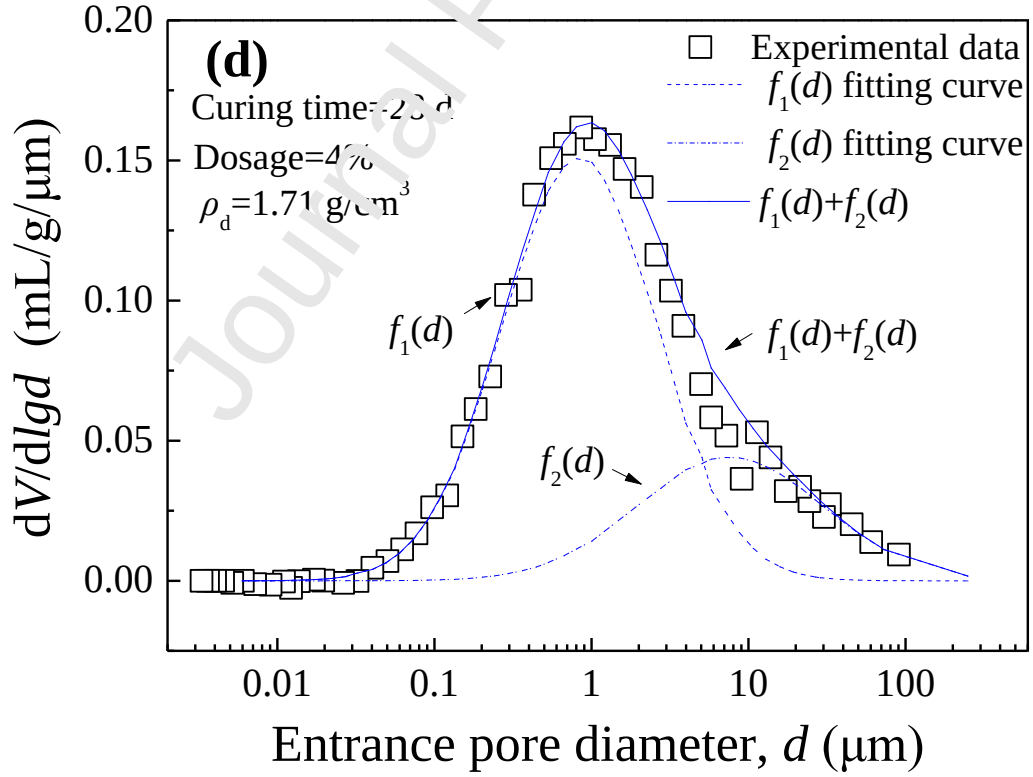

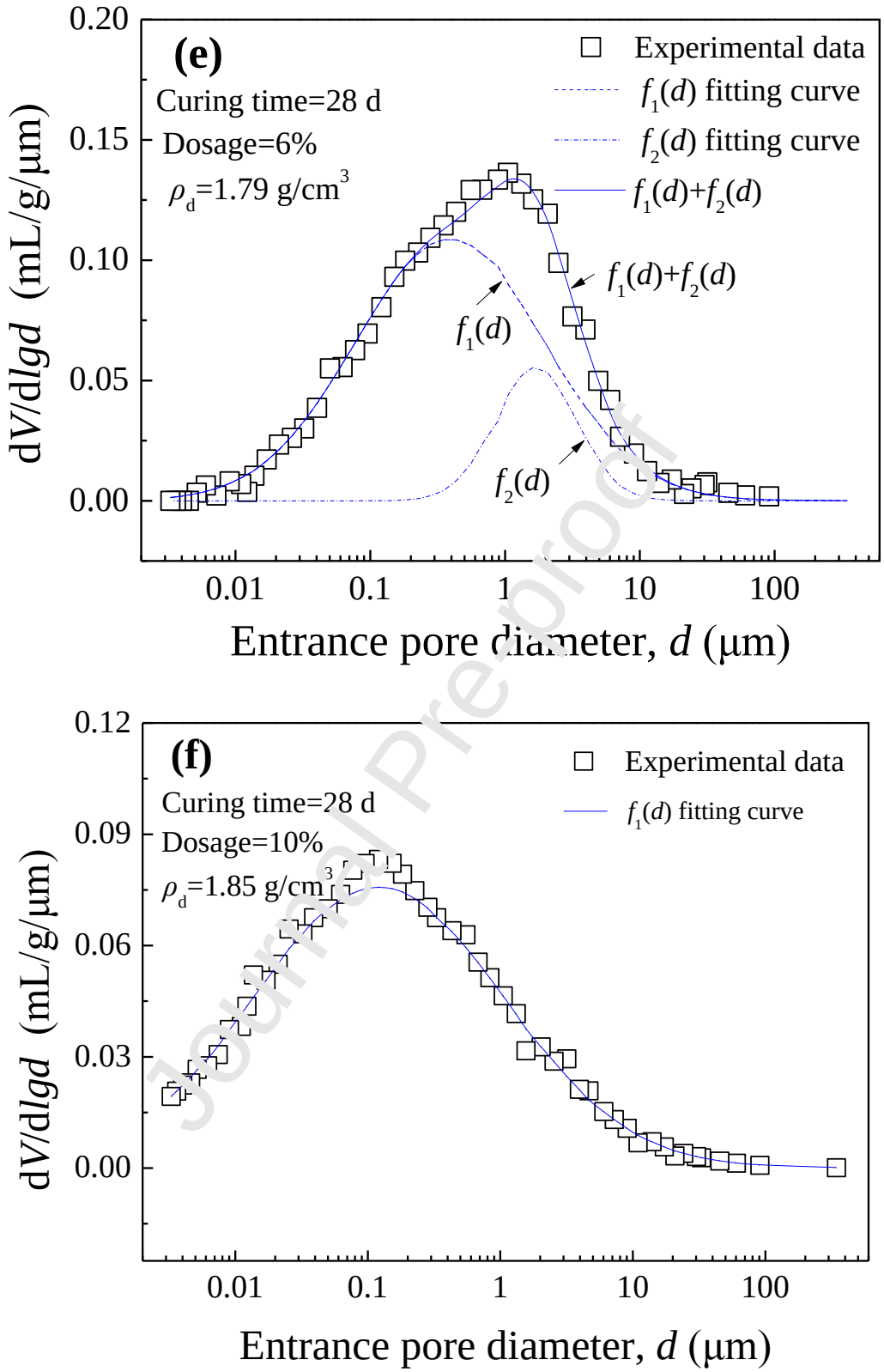

Fig. 7 Variation of pore size distribution and Gaussian fitting curve of solidified/stabilized soil with curing time and binder dosage (Number of replicate = 1).

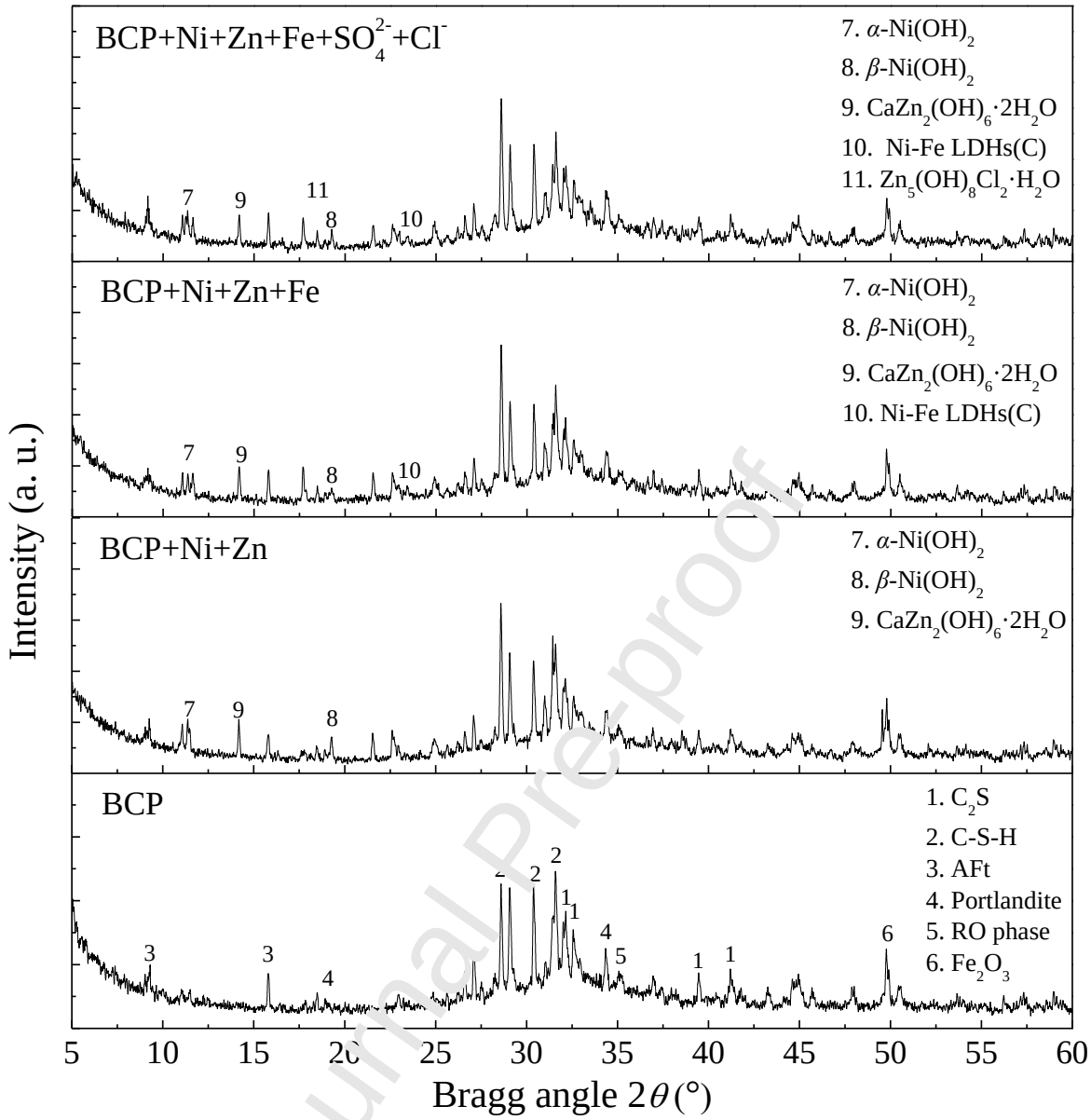

Fig. 8 X-ray diffractograms of BCP binder pastes spiked with different ions contained in contaminated soil. (Number of replicate = 1).

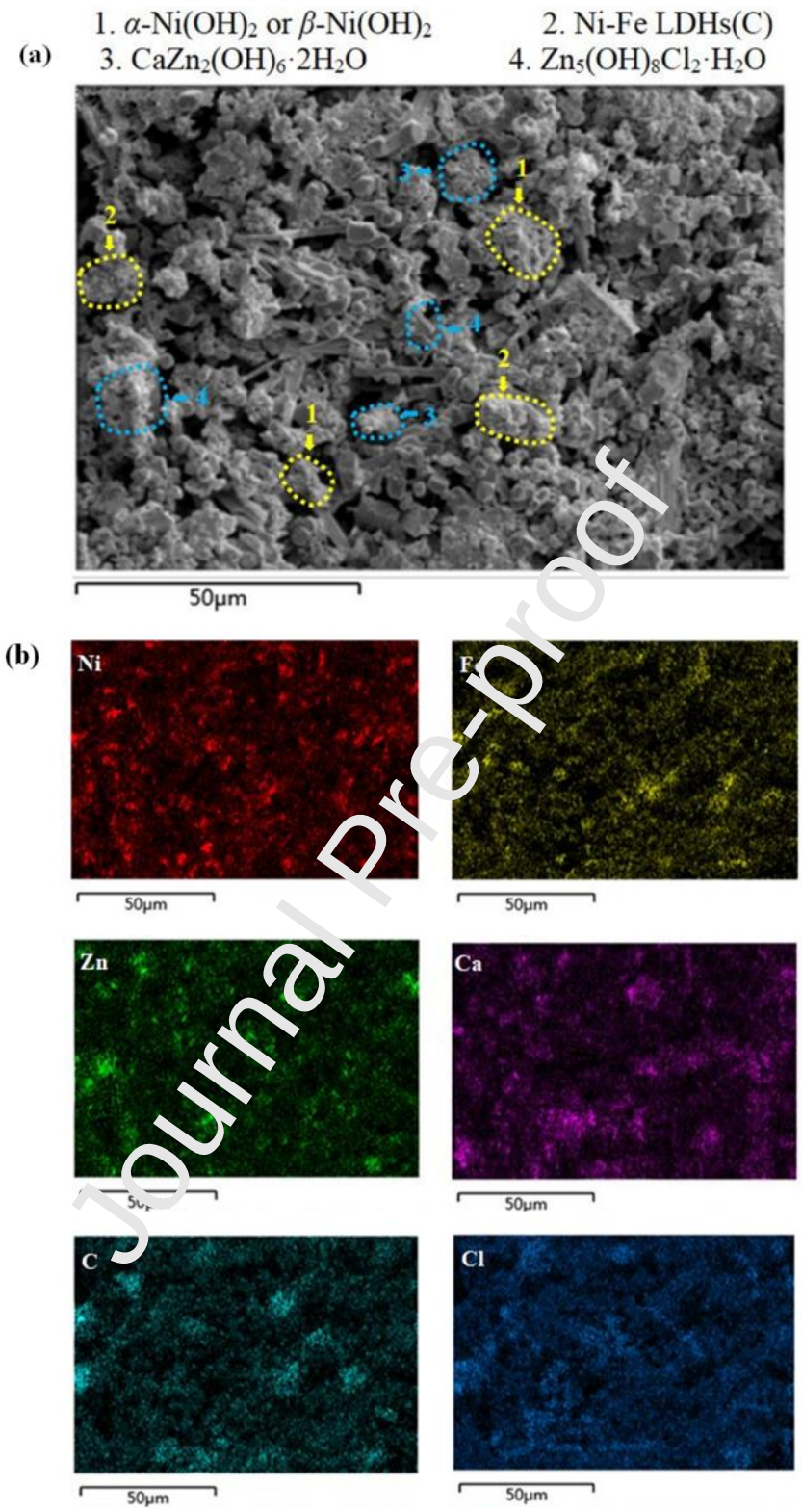

Fig. 9 SEM image of BCP paste spiked with mixture of Ni, Zn, Fe, SO_4^{2-}, and Cl^-, and element distribution map: (Curing time is 28 d and number of replicate = 1).

1. SiO_2; 2. C-S-H; 3. AFt; 4. Portlandite; 5. α-$Ni(OH)_2$; 6. β-$Ni(OH)_2$;
7. Ni-Fe LDHs (S); 8. Ni-Fe LDHs (C); 9. $Zn_5(OH)_8Cl_2 \cdot H_2O$; 10. $CaZn_2(OH)_6 \cdot 2H_2O$

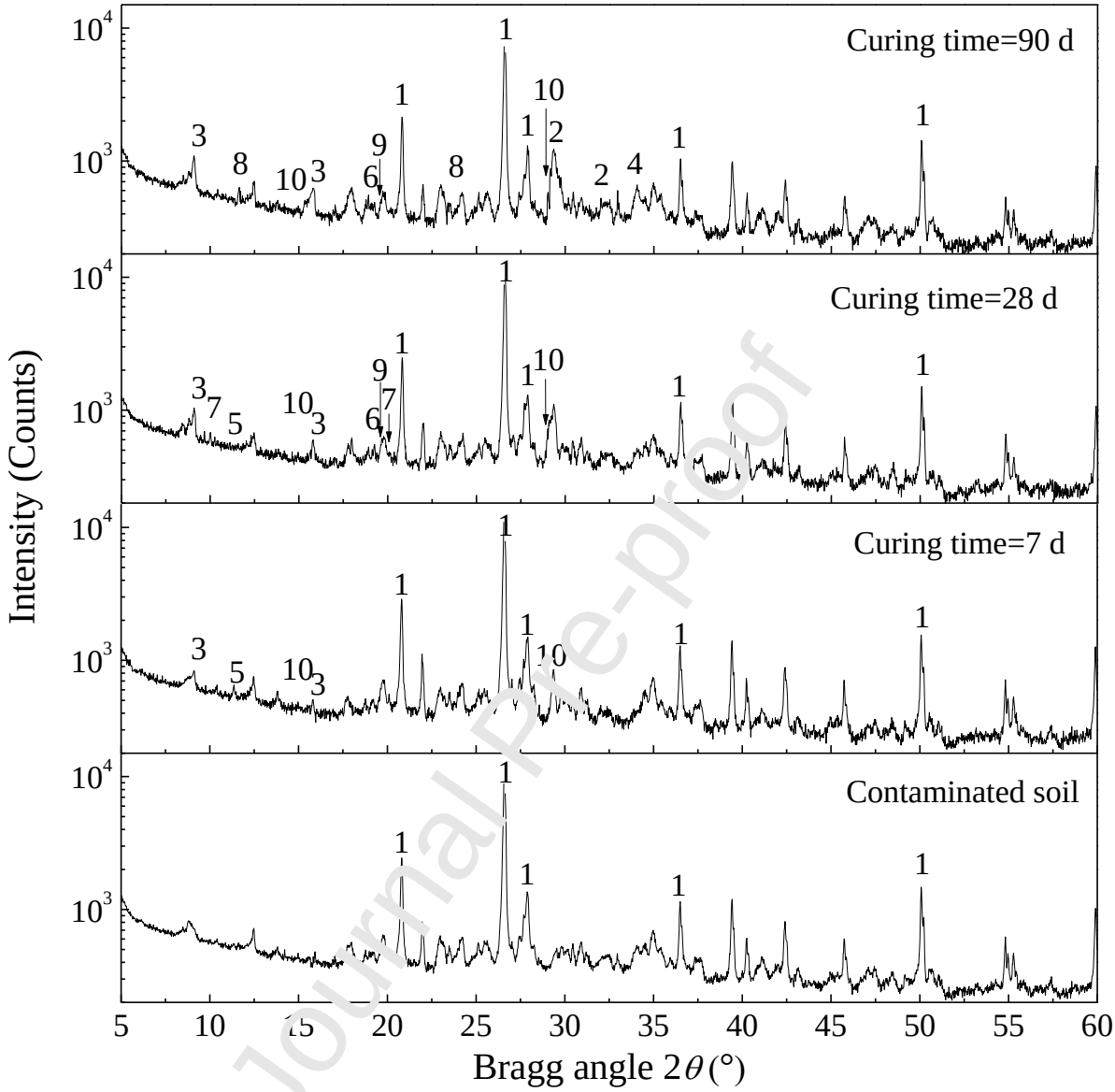

Fig. 10 X-ray diffractograms of the soil solidified/stabilized with 8% BCP dosage at various curing time (Number of replicate = 1).

1. SiO_2; 2. C-S-H; 3. AFt; 4. Portlandite; 5. α-$Ni(OH)_2$; 6. β-$Ni(OH)_2$;
7. Ni-Fe LDHs (S); 8. Ni-Fe LDHs (C); 9. $Zn_5(OH)_8Cl_2 \cdot H_2O$; 10. $CaZn_2(OH)_6 \cdot 2H_2O$

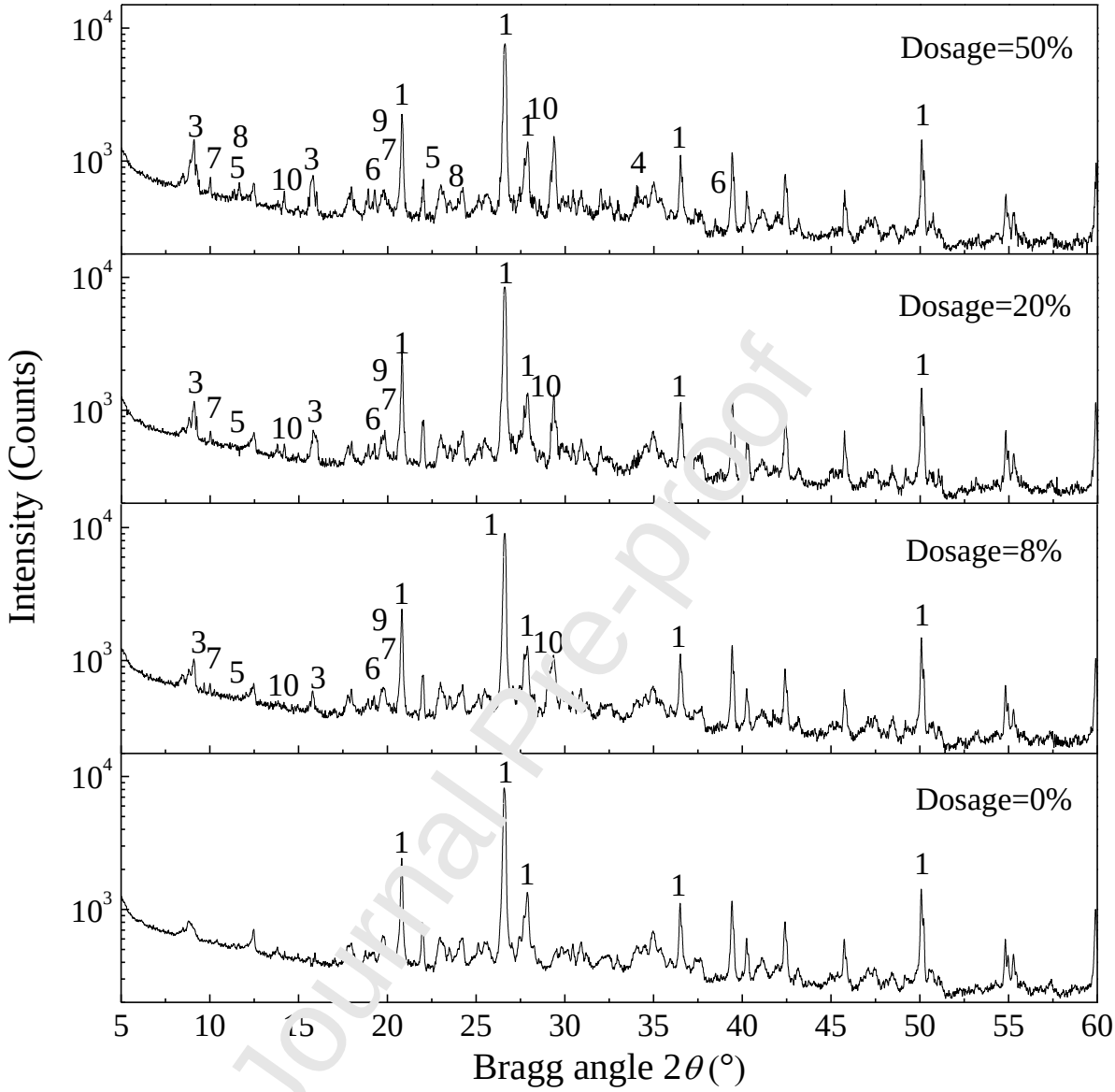

Fig. 11 X-ray diffractograms of the solidified/stabilized soils after 28 d curing with various binder dosages. (Number of replicate = 1).

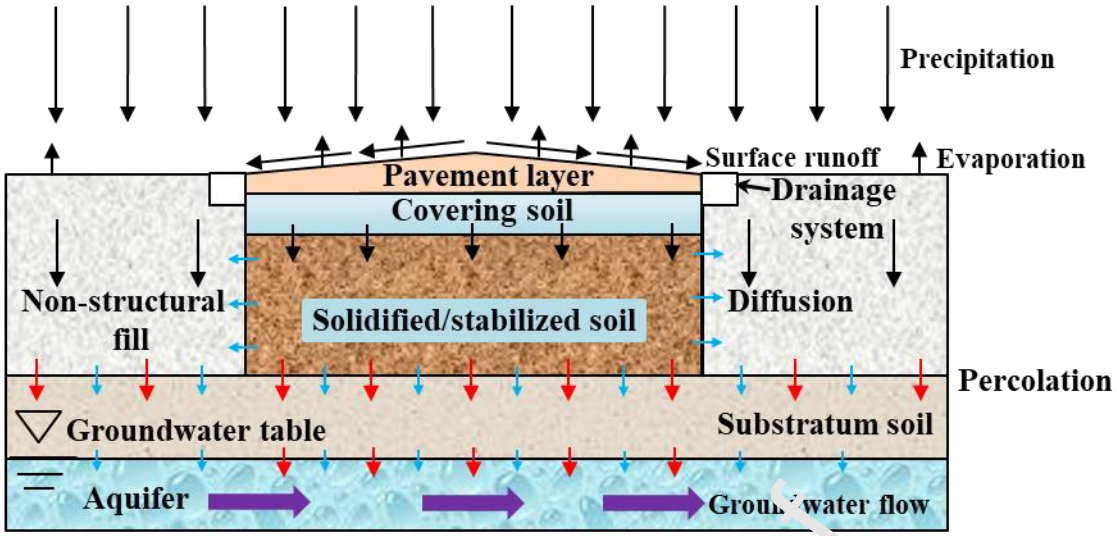

Fig. 12 Water balance and potential environmental impact of contaminants to ambient environment when BCP solidified/stabilized soil is reused as subgrade filling of roadway.

Graphical abstract

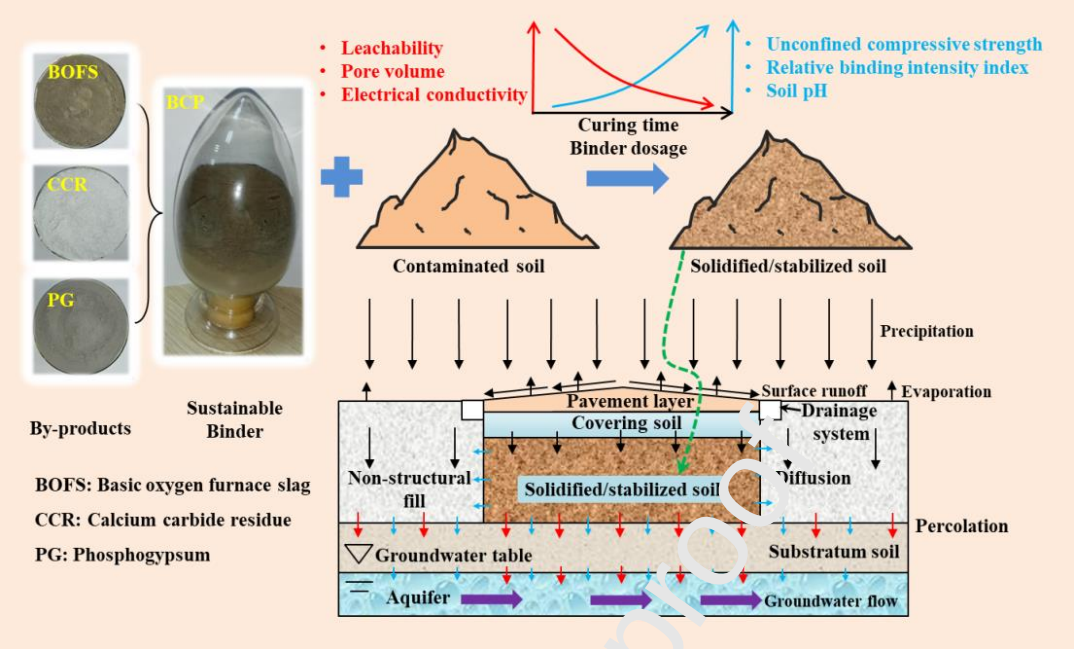

Highlights

BCP, a sustainable by-product-based binder, is developed.

BCP improves the strength but reduces the leachability of contaminated soil.

Solidification and stabilization effectiveness of BCP are investigated.

Curing time and BCP dosage are suggested for soil stabilization/solidification.